JEM Journal of Experimental Medicine

ARTICLE

Ptpn2 and KLRG1 regulate the generation and function of tissue-resident memory CD8⁺ T cells in skin

Katharina Hochheiser[1,2], Florian Wiede[2,3], Teagan Wagner[1], David Freestone[1], Matthias H. Enders[1], Moshe Olshansky[4], Brendan Russ[4], Simone Nüssing[2,5], Emma Bawden[1], Asolina Braun[1], Annabell Bachem[1], Elise Gressier[1], Robyn McConville[1], Simone L. Park[1], Claerwen M. Jones[3], Gayle M. Davey[1], David E. Gyorki[2,6], David Tscharke[7], Ian A. Parish[2,5], Stephen Turner[4], Marco J. Herold[8,9], Tony Tiganis[2,3], Sammy Bedoui[1*], and Thomas Gebhardt[1*]

Tissue-resident memory T cells (T_{RM} cells) are key elements of tissue immunity. Here, we investigated the role of the regulator of T cell receptor and cytokine signaling, Ptpn2, in the formation and function of T_{RM} cells in skin. Ptpn2-deficient CD8⁺ T cells displayed a marked defect in generating CD69⁺ CD103⁺ T_{RM} cells in response to herpes simplex virus type 1 (HSV-1) skin infection. This was accompanied by a reduction in the proportion of KLRG1⁻ memory precursor cells and a transcriptional bias toward terminal differentiation. Of note, forced expression of KLRG1 was sufficient to impede T_{RM} cell formation. Normalizing memory precursor frequencies by transferring equal numbers of KLRG1⁻ cells restored T_{RM} generation, demonstrating that Ptpn2 impacted skin seeding with precursors rather than downstream T_{RM} cell differentiation. Importantly, Ptpn2-deficient T_{RM} cells augmented skin autoimmunity but also afforded superior protection from HSV-1 infection. Our results emphasize that KLRG1 repression is required for optimal T_{RM} cell formation in skin and reveal an important role of Ptpn2 in regulating T_{RM} cell functionality.

Introduction

Peripheral organs and lymphoid tissues harbor large numbers of nonrecirculating memory T cells, many of which are generated in response to pathogens and commensal microbes (Sathaliyawala et al., 2012; Steinert et al., 2015; Gebhardt et al., 2018). These cells are now commonly referred to as tissue-resident memory T (T_{RM}) cells and, over the past decade, have emerged as key mediators of tissue immunity. Accordingly, T_{RM} cells afford rapid and potent protection from viral, bacterial, fungal, and parasitic pathogens and drive local control of latent-reactivating and persisting infections (Park and Kupper, 2015; Gebhardt et al., 2018). Recent preclinical and translational studies have further implicated T_{RM} cells in tumor control and response to checkpoint blockade immunotherapy, with elevated numbers of T_{RM} cells linked to better patient survival across a broad spectrum of cancers (Smazynski and Webb, 2018; Park et al., 2019b). Aberrant T_{RM} responses, on the other hand, are associated with tissue pathology in the context of autoimmune inflammation, allergy, and transplant rejection (Clark, 2015; Park and Kupper, 2015; Turner et al., 2014). Thus, the therapeutic manipulation of T_{RM} responses carries great potential for the prevention and treatment of a broad spectrum of diseases. Any such attempts, however, will require a profound understanding of the molecular mechanisms that operate during the formation and maintenance of T_{RM} cells and that determine their function.

The epithelial layers of skin, small intestinal mucosa, and other organs are populated by CD8⁺ T_{RM} cells that commonly express surface markers such as CD69 and CD103 and share core transcriptional signatures that distinguish them from recirculating T cells (Mackay et al., 2016; Mackay et al., 2013).

[1]Department of Microbiology & Immunology, The University of Melbourne at the Peter Doherty Institute for Infection & Immunity, Melbourne, Victoria, Australia; [2]Peter MacCallum Cancer Centre Melbourne, Melbourne, Victoria, Australia; [3]Monash Biomedicine Discovery Institute, Department of Biochemistry and Molecular Biology, Monash University, Clayton, Victoria, Australia; [4]Department of Microbiology, Monash University, Clayton, Victoria, Australia; [5]Sir Peter MacCallum Department of Oncology, The University of Melbourne, Parkville, Victoria, Australia; [6]Department of Surgery, University of Melbourne, Parkville, Victoria, Australia; [7]The John Curtin School of Medical Research, The Australian National University, Acton, Australian Capital Territory, Australia; [8]The Walter & Eliza Hall Institute for Medical Research, Parkville, Victoria, Australia; [9]Department of Medical Biology, University of Melbourne, Parkville, Victoria, Australia.

*S. Bedoui and T. Gebhardt contributed equally to this paper; Correspondence to Thomas Gebhardt: gebhardt@unimelb.edu.au; Katharina Hochheiser: katharina.hochheiser@unimelb.edu.au.

These T_{RM} cells can develop from precursors found within the killer cell lectin-like receptor G1 (KLRG1)–negative pool of $CD8^+$ T cells expanded in response to acute pathogen encounter (Mackay et al., 2013; Sheridan et al., 2014), although a recent study using a fate-mapping fluorescent reporter system indicated that some effector $CD8^+$ T cells may switch off KLRG1 expression and give rise to various subsets of memory cells, including T_{RM} cells (Herndler-Brandstetter et al., 2018). Regardless, in the case of viral skin infection, $CD69^+$ $KLRG1^-$ effector cells are highly enriched in the epidermis early after onset of T cell infiltration, while at the same time their $KLRG1^+$ counterparts dominate the effector pool in spleen and blood (Mackay et al., 2013). Thus, selective accumulation of $CD69^+$ $KLRG1^-$ cells in the epidermal layer establishes an early local pool of effector cells with potential to differentiate into $CD69^+$ $CD103^+$ T_{RM} cells upon resolution of infection. Interestingly, both KLRG1 and the αEβ7 integrin (the latter incorporating the αE subunit CD103) share one of their major ligands, E-cadherin, a molecule expressed not only by epithelial cells, such as keratinocytes and Langerhans cells (Gründemann et al., 2006), but also by T_{RM} cells (Hofmann and Pircher, 2011; Mackay et al., 2013). While both CD103 and E-cadherin can promote T_{RM} cell formation and maintenance (Casey et al., 2012; Hofmann and Pircher, 2011; Mackay et al., 2013; Sheridan et al., 2014), it has remained unclear if simultaneous repression of KLRG1 expression is also necessary for the establishment of T_{RM} cells.

The extent to which T_{RM} cells are generated following skin infection is determined by diverse factors and interconnected molecular processes, including the generation of $KLRG1^-$ T_{RM} cell precursors in skin-draining lymph nodes, precursor infiltration of peripheral tissues, local antigen reencounter, repression of tissue exit receptors, chemokine-directed epidermal migration, and, critically, exposure to locally produced cytokines such as TGFβ and IL-15 (Gebhardt et al., 2018). These processes are regulated and fine-tuned at the molecular level as to ensure transition into long-lived memory cells and adjustment of T_{RM} cell functionality according to the tissue of residence. The protein tyrosine phosphatase nonreceptor type 2 (Ptpn2) is an important negative regulator of $CD8^+$ T cell responses in the context of autoimmunity, lymphopenia, cancer, and chronic infection (LaFleur et al., 2019; Wiede et al., 2014a; Wiede et al., 2020; Wiede et al., 2011; Wiede et al., 2014b). Ptpn2 attenuates TCR signaling by dephosphorylating TCR-proximal kinases, such as LCK and FYN, which results in an increased T cell activation threshold and, consequently, reduced responsiveness to low-affinity antigen (Wiede et al., 2011; Wiede et al., 2014a; Wiede et al., 2014b). Furthermore, Ptpn2 dephosphorylates and inactivates components of the JAK-STAT signaling pathways, thereby attenuating cytokine signaling employed by members of the IFN and common γ-chain cytokine families, such as type I and II IFN, IL-2, IL-15, and others (Simoncic et al., 2002; Aoki and Matsuda, 2002; Wiede et al., 2011; Wiede et al., 2014a; ten Hoeve et al., 2002; LaFleur et al., 2019). Thus, Ptpn2 appears likely to operate as a rheostat for T_{RM} cell development and function, although its role in T_{RM} cell biology has remained largely unexplored.

Here, we investigated the role of Ptpn2 in T_{RM} cell formation using a model of acute HSV skin infection. We describe that absence of Ptpn2 expression in $CD8^+$ T cells results in perturbed effector differentiation with predominant production of short-lived $KLRG1^+$ effectors and impaired generation of epidermal T_{RM} cells. Interestingly, forced expression of KLRG1 alone compromises T_{RM} development, while $KLRG1^-$ effector cells with memory potential develop normally into T_{RM} cells independently of Ptpn2 expression. Finally, we show that Ptpn2 is expressed by resting T_{RM} cells and functions to restrict T_{RM} responses to both virus infection and innocuous model antigens. Thus, our study describes the molecules Ptpn2 and KLRG1 as new regulatory factors for the development and function of T_{RM} cells and highlights the potential of therapeutic inhibition of Ptpn2 activity as a way to amplify T_{RM} cell–mediated immunity.

Results

Impaired T_{RM} cell formation by Ptpn2-deficient $CD8^+$ T cells in response to HSV infection

To test whether Ptpn2 impacted $CD8^+$ T cell responses to an acute viral infection, we tracked Ova-specific $CD8^+$ T (OT-I) cells adoptively transferred into mice infected on the skin with an HSV-1 strain expressing the model antigen Ova (HSV-Ova). In this setting, naive OT-I cells generate strong effector responses that ultimately give rise to recirculating memory T cells as well as long-lived $CD69^+CD103^+$ T_{RM} cells concentrated at the site of resolved infection (Mackay et al., 2013). To allow for endogenous T cell responses to commence unperturbed and thus provide a level of competition with the transgenic T cells, which we presumed would best reveal any regulatory impact of Ptpn2 on $CD8^+$ T cell expansion and activation, we transferred control (*Ptpn2*$^{fl/fl}$) or genetically Ptpn2-deficient (*Lck*-Cre;*Ptpn2*$^{fl/fl}$) naive OT-I cells 2 d after infection (Wiede et al., 2011). While both populations expanded robustly, numbers of OT-I.*Lck*-Cre;*Ptpn2*$^{fl/fl}$ cells recovered from spleen 1 and 2 wk after infection were increased on average by ∼2.7- and 3.7-fold compared with mice that received control OT-I.*Ptpn2*$^{fl/fl}$ cells, respectively (Fig. 1 A). Numbers of OT-I cells recovered from the spleen were very low for both genotypes at later time points. By contrast, fewer OT-I.*Lck*-Cre;*Ptpn2*$^{fl/fl}$ than OT-I.*Ptpn2*$^{fl/fl}$ cells were recovered from skin at 2 and 4 wk after inoculation when virus infection had resolved (van Lint et al., 2004; Fig. 1 A). This reduction in numbers was particularly evident for the population of $CD69^+$ $CD103^+$ T_{RM} cells that evolved with slower kinetics and overall less efficiency from Ptpn2-deficient OT-I cells compared with control OT-I cells (Fig. 1, A and B). In line with this, histological examination and flow cytometric enumeration of OT-I cells in mechanically separated epidermis and dermis revealed that OT-I.*Lck*-Cre;*Ptpn2*$^{fl/fl}$ cells were sparse in the epithelial compartments where $CD69^+$ $CD103^+$ skin T_{RM} cells arise (i.e., epidermis and hair follicle epithelium; Gebhardt et al., 2009; Mackay et al., 2013; Fig. 1, A, C, and D). This apparent defect in epidermal entry and/or retention did not appear to be caused by an inability of Ptpn2-deficient OT-I cells to respond to the T_{RM}-instructive factor TGFβ, as both OT-I.*Lck*-Cre;*Ptpn2*$^{fl/fl}$ and control OT-I cells activated by peptide-pulsed splenocytes in vitro strongly up-regulated CD103 in response to this cytokine (Fig. S1 A).

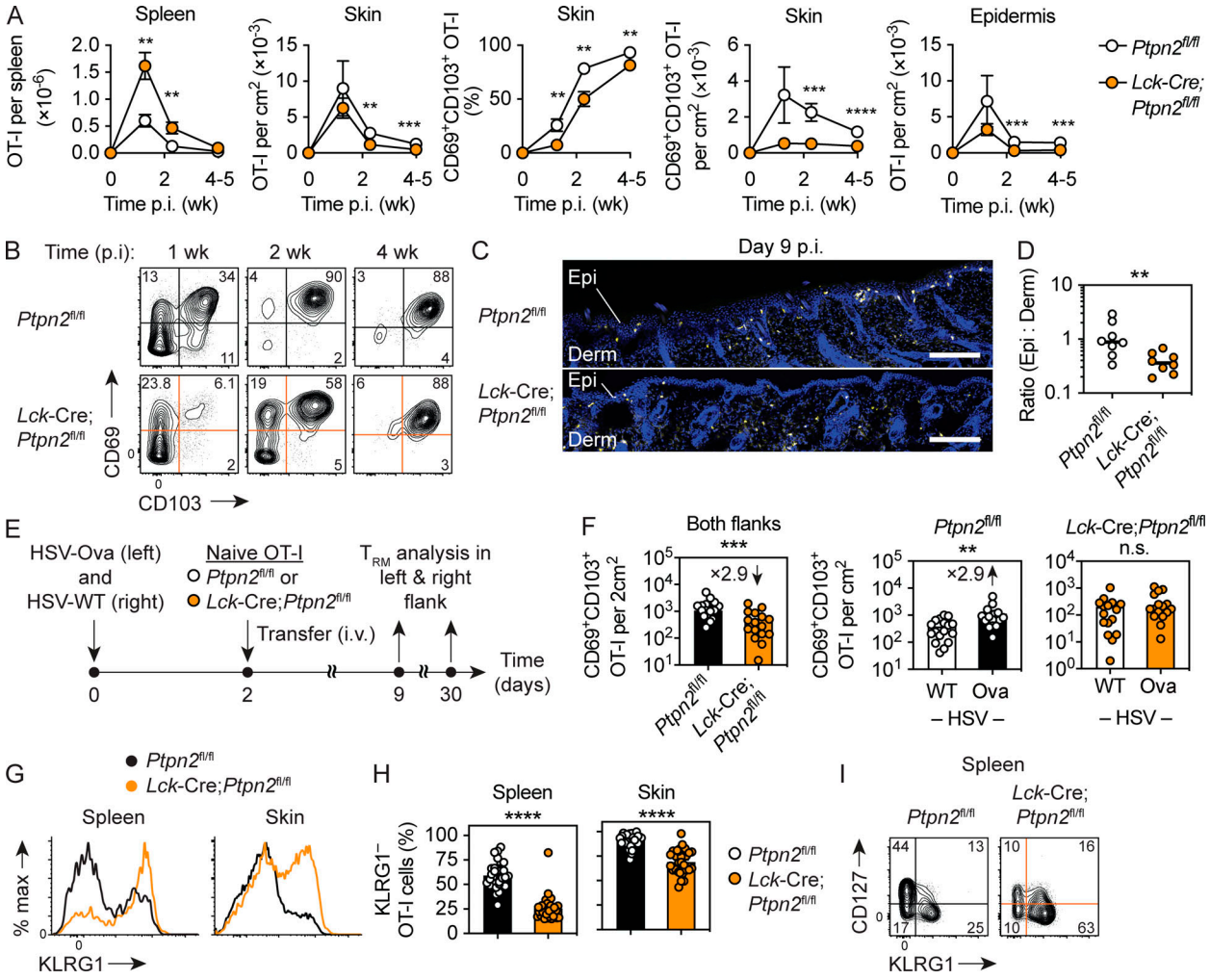

Figure 1. **Absence of Ptpn2 promotes the generation of KLRG1⁺ effector cells and impairs T_{RM} cell formation in response to HSV skin infection.** **(A–C)** WT CD45.1⁺ mice were infected with HSV-Ova and 2 d later received naive *Ptpn2*$^{fl/fl}$ (white) or *Lck*-Cre;*Ptpn2*$^{fl/fl}$ (orange) CD45.2⁺ OT-I cells (5 × 10⁴ i.v.). **(A)** Enumeration of total and CD69⁺ CD103⁺ OT-I cells in spleen, skin, and epidermis by flow cytometry at indicated times post infection (p.i). Data pooled from *n* = 2 experiments with *n* = 8–9 mice/time point/group (mean ± SEM). **(B)** Analysis of CD69 and CD103 expression by OT-I cells in skin. **(C and D)** Immunofluorescence analysis of skin sections stained with Hoechst 33342 (blue) and anti-CD45.2 antibody to detect OT-I cells (yellow). Scale bars, 200 µm. Data in D were pooled from *n* = 2 experiments with *n* = 8 mice in total. Derm, dermis; Epi, epidermis. **(E)** WT CD45.1⁺ mice were infected with both HSV-Ova (left flank) and WT HSV (right flank) and 2 d later received congenic naive *Ptpn2*$^{fl/fl}$ (white) or *Lck*-Cre;*Ptpn2*$^{fl/fl}$ (orange) CD45.2⁺ OT-I cells (5 × 10⁴ i.v.). **(F)** Enumeration of CD69⁺ CD103⁺ OT-I T_{RM} cells in skin 30 d p.i.; data were pooled from *n* = 3 experiments with *n* = 16–17 mice/group. **(G–I)** Analysis of KLRG1 and (I) CD127 expression by *Ptpn2*$^{fl/fl}$ and *Lck*-Cre;*Ptpn2*$^{fl/fl}$ OT-I cells in spleen and skin 9 d p.i.; data in H pooled from *n* = 7 experiments with *n* = 31 mice/group. Statistical significance (**, P < 0.01; ***, P < 0.001; ****, P < 0.0001) determined by Mann–Whitney test for individual time points. Derm, dermis; Epi, epidermis.

Recognition of cognate antigen in infected skin promotes the formation of T_{RM} cells, although the molecular mechanisms involved are only incompletely understood (Gebhardt et al., 2009; Khan et al., 2016; Muschaweckh et al., 2016). Given the established function of Ptpn2 in dampening TCR signaling, we asked whether local antigen recognition in infected skin impacted T_{RM} cell formation by OT-I.*Lck*-Cre;*Ptpn2*$^{fl/fl}$ cells. To this end, we infected mice with both HSV-Ova and WT HSV-1 (HSV-WT, not expressing Ova) strains on opposite flanks, followed by transfer of naive OT-I.*Lck*-Cre;*Ptpn2*$^{fl/fl}$ or control OT-I.*Ptpn2*$^{fl/fl}$ cells (Fig. 1 D). Confirming our previous result from a single infection, OT-I.*Lck*-Cre;*Ptpn2*$^{fl/fl}$ cells generated fewer CD69⁺ CD103⁺ T_{RM} cells across both flanks when analyzed 30 d later (Fig. 1 E). As expected, antigen presence increased CD69⁺ CD103⁺ T_{RM} cell formation by control OT-I.*Ptpn2*$^{fl/fl}$ cells (Fig. 1 E). By contrast, Ptpn2-deficient OT-I cells generated comparable numbers of T_{RM} cells in the presence (HSV-Ova) or absence (HSV-WT) of local antigen (Fig. 1 E). Thus, Ptpn2-deficient effector cells infiltrating infected skin failed to respond to important environmental cues such as local antigen stimulation to support the formation of long-lived epidermal memory cells. Interestingly, skin epithelial-infiltrating CD103⁺ OT-I.*Lck*-Cre;*Ptpn2*$^{fl/fl}$ cells were similarly reduced in the presence (HSV-Ova) or absence (HSV-WT) of antigen early after infection (day 9; Fig. S1 B). This defect likely reflected a more general impairment in overall memory potential in the pool of Ptpn2-deficient effector cells infiltrating infected skin, independent of potentially negative effects of excessive local TCR stimulation on memory formation in absence of

Ptpn2. Regardless, the results thus far established that OT-I.*Lck*-Cre;*Ptpn2*$^{fl/fl}$ cells were impaired in forming epidermal CD69$^+$ CD103$^+$ T_{RM} cells in response to an acute skin infection.

Ptpn2 regulates the accumulation of KLRG1$^-$ effector CD8$^+$ T cells in skin

The surface molecules CD127 (IL-7Rα) and KLRG1 are often used as markers to predict the memory potential of activated CD8$^+$ T cells, with short-lived effector cells identified as CD127^{lo} KLRG1$^+$ and long-lived memory precursors as CD127^{hi} KLRG1$^-$ cells (Joshi et al., 2007; Sarkar et al., 2008), the latter of which also contain cells that can give rise to CD69$^+$ CD103$^+$ T_{RM} cells (Mackay et al., 2013; Sheridan et al., 2014). Given that Ptpn2 has recently been identified as a regulator of CD8$^+$ T cell expansion and differentiation during systemic infection (LaFleur et al., 2019; Flosbach et al., 2020), we next compared the phenotype of effector T cells arising in the presence or absence of Ptpn2 expression around the peak of expansion after acute peripheral infection. Flow cytometric analysis of OT-I cells isolated from spleens 9 d after HSV single or double infection revealed a marked reduction in the frequency of KLRG1$^-$ and CD127^{hi} memory precursors among *Lck*-Cre;*Ptpn2*$^{fl/fl}$ cells when compared with *Ptpn2*$^{fl/fl}$ controls (Fig. 1, G–I), although the absolute numbers of KLRG1$^-$ effector cells did not differ between the two genotypes (Fig. S1 C). The decrease in the proportion of KLRG1$^-$ *Lck*-Cre;*Ptpn2*$^{fl/fl}$ OT-I cells in spleen was also evident in infected skin. Whereas the vast majority of *Ptpn2*$^{fl/fl}$ control cells in skin displayed a KLRG1$^-$ phenotype (91.2 ± 1.7%), as previously reported (Mackay et al., 2013), *Lck*-Cre;*Ptpn2*$^{fl/fl}$ OT-I cells comprised a ∼2:1 mixture of KLRG1$^-$ and KLRG1$^+$ cells (Fig. 1, G and H). This was echoed by an on average 2.4-fold reduction of KLRG1$^-$ *Lck*-Cre;*Ptpn2*$^{fl/fl}$ OT-I cells compared with control *Ptpn2*$^{fl/fl}$ OT-I effector cells in skin (Fig. S1 D). Thus, absence of Ptpn2 expression promoted the expansion and differentiation of KLRG1$^+$ CD127^{lo} effector cells, which caused an increase in the proportion of KLRG1$^+$ cells in infected skin and an accompanying reduction in numbers of KLRG1$^-$ cells.

Forced expression of KLRG1 impedes T_{RM} cell formation

In combination with other markers, KLRG1 is often used as a surrogate for terminally differentiated effector T cells with limited proliferative and memory potential (Joshi et al., 2007; Sarkar et al., 2008; Voehringer et al., 2001; Voehringer et al., 2002), although its functional role in the development of recirculating memory cells after systemic infection appears to be minimal (Gründemann et al., 2010). T_{RM} cells in the epidermal layer of skin develop from KLRG1$^-$ precursors, and these dominate the epidermal-infiltrating effector population from the earliest times after infection (Mackay et al., 2013), implying selective entry of KLRG1$^-$ cells and/or suppression of KLRG1 expression by locally produced factors such as TGFβ (Schwartzkopff et al., 2015). Of note, KLRG1 and the $\alpha_E\beta_7$ integrin (incorporating the α_E-chain CD103) both bind to E-cadherin expressed by epithelial cells such as keratinocytes (Cepek et al., 1994; Gründemann et al., 2006; Hofmann and Pircher, 2011), and both CD103 and E-cadherin are required for optimal generation of T_{RM} cells in a number of organs (Casey et al., 2012; Hofmann and Pircher, 2011; Mackay et al., 2013; Sheridan et al., 2014). Therefore, we speculated that T_{RM} cell generation might rely on repression of KLRG1 expression, which in part could have explained our findings with *Lck*-Cre;*Ptpn2*$^{fl/fl}$ OT-I cells.

To address this, we transduced in vitro activated TCR-transgenic CD8$^+$ T cells (gBT-I) specific for a HSV-derived epitope in glycoprotein B (gB) with a retroviral vector encoding for KLRG1 and GFP (pMIG.*Klrg1*-WT; Fig. 2 A). As a control, gBT-I cells were transduced with a control vector encoding GFP, but not KLRG1 (pMIG.Ctrl). Of note, T cell activation with gB peptide–pulsed splenocytes in presence of IL-2 yields activated gBT-I cells with considerable potential to form long-lived memory cells (Mackay et al., 2012) and does not induce KLRG1 expression in the absence of IL-12 supplementation. Accordingly, KLRG1-transduced cells expressed KLRG1 on their surface, whereas cells transduced with the control vector were negative for KLRG1 expression (Fig. 2 B). On day 3 after transduction, GFP$^+$ gBT-I cells were sorted and transferred into mice, followed by treatment of flank skin with 1-fluor-2,4-dinitrobenzol (DNFB) to attract cells into the skin for T_{RM} cell formation, as previously described (Mackay et al., 2012). 4 wk after DNFB treatment, we recovered similar numbers of KLRG1-overexpressing and control gBT-I cells from spleen (Fig. 2 C). By contrast, KLRG1-expressing gBT-I cells in the DNFB-treated skin, and in particular CD69$^+$ CD103$^+$ T_{RM} cells, were significantly reduced (Fig. 2 C).

To test whether forced KLRG1 expression also affected T_{RM} cell formation in response to skin infection, we generated bone marrow chimeric mice as a source of naive pMIG.*Klrg1*-overexpressing and control gBT-I cells by reconstituting lethally irradiated mice with gBT-I bone marrow cells transduced with pMIG.*Klrg1*-WT or pMIG control vectors (Fig. 2 D). 8 wk after bone marrow transfer, KLRG1 expression by gBT-I cells in the chimeras was confirmed by surface staining (Fig. 2 E). Naive GFP$^+$ gBT-I cells were isolated and sorted from lymph nodes and spleens and transferred into recipient mice 1 d after HSV skin infection (Fig. 2 D). Analysis of GFP$^+$ gBT-I cells >4 wk after infection revealed a modest 1.4-fold increase of pMIG.*Klrg1*-WT transduced gBT-I cells in spleen, whereas CD69$^+$ CD103$^+$ T_{RM} cell numbers and frequencies in skin were significantly reduced (Fig. 2, F and G). KLRG1 expression levels in splenic gBT-I cells were comparable to expression levels found on control effector gBT-I cells, largely excluding that nonphysiological KLRG1 expression levels may have caused impaired T_{RM} cell formation (Fig. 2 E). Furthermore, the vast majority of pMIG.*Klrg1*-WT transduced gBT-I cells in spleen retained high KLRG1 surface expression (Fig. 2 F). By contrast, their T_{RM} cell counterparts in skin displayed evidence for partial down-modulation of KLRG1 expression both at the population and single-cell level (Fig. 2 F), implying selection pressure against KLRG1 expression specifically for T_{RM} cells. Combined, these results established that forced expression of KLRG1 inhibited T_{RM} cell formation in skin in settings of inflammation and viral infection.

KLRG1-mediated inhibition of T_{RM} cell formation involves immunoreceptor tyrosine–based inhibitory motif (ITIM) signaling

We next set out to address the mechanisms by which KLRG1 can inhibit T_{RM} cell formation in skin. Previous studies have shown

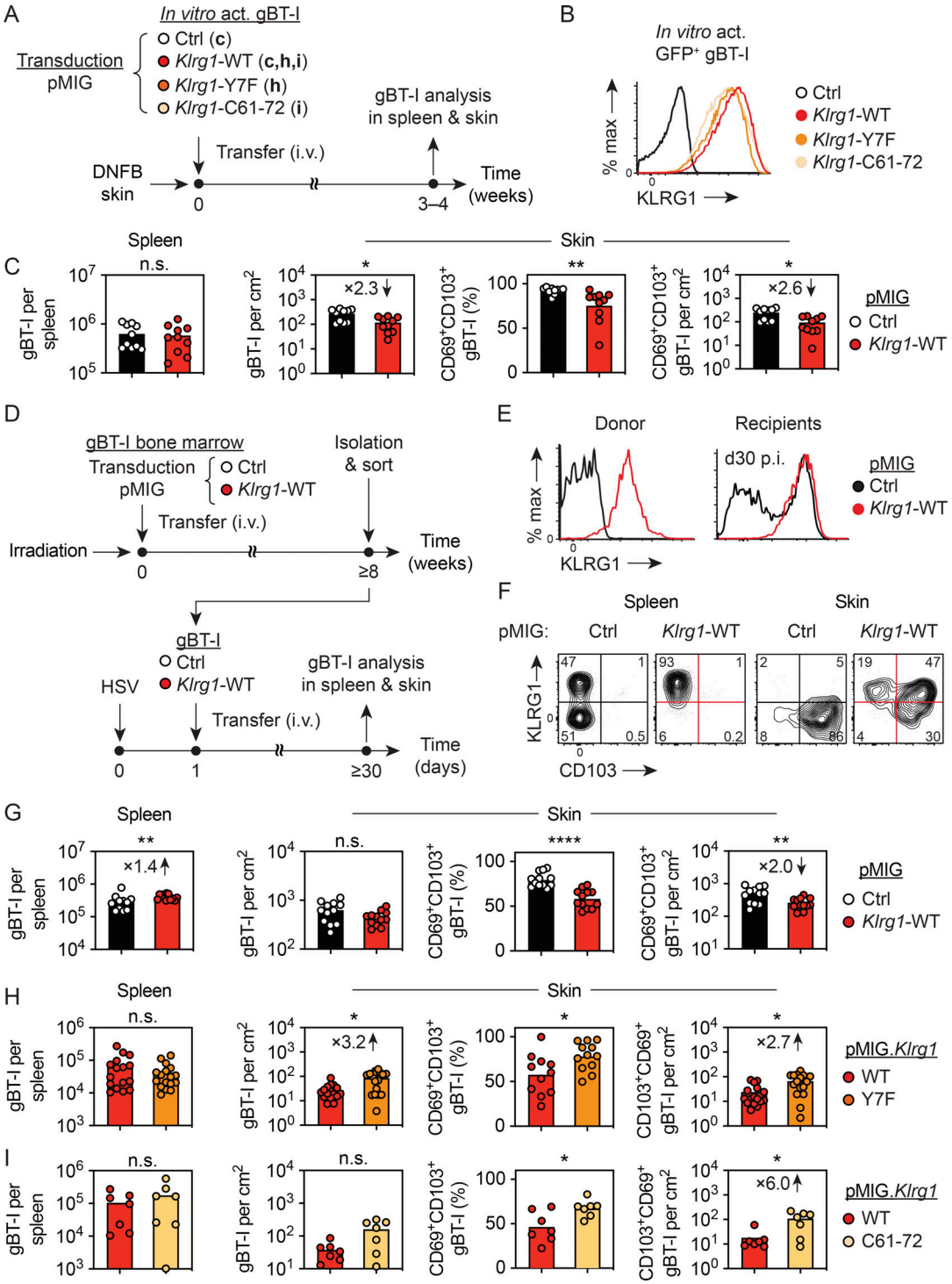

Figure 2. **Forced KLRG1 expression impedes T_{RM} cell formation in skin. (A)** gBT-I cells were activated in vitro and transduced with a control vector (pMIG.Ctrl) or vectors coding for WT (pMIG.*Klrg1*.WT) or mutant (pMIG.*Klrg1*.Y7F; pMIG.*Klrg1*.C61-72) KLRG1. Sorted GFP$^+$ cells were i.v. transferred (2.5 × 10^6 in C; 1 × 10^6 in H and I) into WT mice treated on flank skin with DNFB and gBT-I cells in spleen and skin analyzed 3–4 wk later. **(B)** Analysis of KLRG1 expression by transduced GFP$^+$ gBT-I cells before transfer. **(C)** Enumeration of total and CD69$^+$ CD103$^+$ gBT-I cells in spleen and skin 4 wk after transfer (pMIG.Ctrl, white; pMIG.*Klrg1*.WT, red). Data pooled from *n* = 2 experiments with *n* = 10 mice per group. **(D–G)** Bone marrow cells from gBT-I mice were transduced with pMIG.Ctrl or pMIG.*Klrg1*.WT and transferred into lethally irradiated WT mice. Following reconstitution, GFP^{hi} KLRG1^{hi} Vα2$^+$ CD8$^+$ gBT-I cells were isolated, sorted, and transferred (2–10 × 10^4 i.v.) into congenic mice infected with HSV-WT 1 d earlier. **(E)** Analysis of KLRG1 expression by GFP$^+$ gBT-I cells from donor and recipient mice (pMIG.Ctrl, black; pMIG.*Klrg1*.WT, red). **(F and G)** Analysis of KLRG1 and CD103 expression by gBT-I cells in spleen and skin (F; numbers indicate percentage in each quadrant) and enumeration of total and CD69$^+$ CD103$^+$ gBT-I cells 4 wk after infection (G). Data pooled from *n* = 2 experiments with *n* = 12 mice/group. Ctrl, control. **(H and I)** gBT-I cells were transduced with pMIG.*Klrg1*.WT (red), pMIG.*Klrg1*.Y7F (orange), or pMIG.*Klrg1*.C61-72 (light orange) and transferred into DNFB-treated recipients as described in A. Enumeration of total and CD69$^+$CD103$^+$ GFP$^+$ gBT-I cells in spleen and skin 3 wk after transfer. Data pooled from *n* = 4 experiments with *n* = 15–17 mice/group (H) or from *n* = 2 experiments with *n* = 7 mice/group (I). Statistical significance (*, P < 0.05; **, P < 0.01; ****, P < 0.0001) determined by Mann–Whitney test.

that KLRG1 and CD103 are mutually exclusively expressed in the majority of effector CD8⁺ T cells infiltrating infected skin and intestinal mucosa (Mackay et al., 2013; Sheridan et al., 2014). Therefore, we speculated that forced expression of KLRG1 may impact CD103 expression and tested this by exposing KLRG1-overexpressing cells to TGFβ in vitro. Nevertheless, we found normal CD103 up-regulation, ruling out a general defect in expression of this integrin subunit by KLRG1⁺ cells (Fig. S1 E). Binding of KLRG1 to E-cadherin induces an ITIM–mediated signaling cascade that results in inhibition of TCR signaling and T cell proliferation (Beyersdorf et al., 2001; Tessmer et al., 2007; Henson et al., 2009). To test whether KLRG1-ITIM signaling was involved in the inhibition of T_{RM} cell formation, we transduced gBT-I cells with vectors encoding for signaling-deficient KLRG1 proteins and tested their ability to form T_{RM} cells as above (Fig. 2 A). KLRG1-Y7F harbors a point mutation in its ITIM that abrogates recruitment of phosphatases and consequently results in reduced inhibitory capacity (Tessmer et al., 2007; Rosshart et al., 2008). KLRG1-C61-72 harbors four point mutations replacing cysteines in its stalk region crucial for multimerization, which prevents multivalent E-cadherin binding and inhibitory signaling (Hofmann et al., 2012). Flow cytometric analysis confirmed KLRG1 expression on GFP⁺ cells transduced with WT KLRG1, KLRG1-Y7F, and KLRG1-C61-72, although we noted somewhat lower expression of KLRG1-Y7F and KLRG1-C61-72 compared with KLRG1-WT (Fig. 2 B). 3 wk after transfer and skin treatment with DNFB, similar numbers of all types of gBT-I cells were recovered from spleens (Fig. 2, H and I). By contrast, gBT-I cells expressing ITIM mutant or multimerization-deficient KLRG1 molecules displayed a heightened capacity to generate T_{RM} cells, which manifested in increased numbers and frequencies of CD69⁺ CD103⁺ cells in skin compared with gBT-I cells expressing WT KLRG1 (Fig. 2, H and I). These results implied that signaling via ITIM in the cytoplasmatic domain of KLRG1 was involved in inhibiting T_{RM} cell formation in the skin, and they inferred that increased KLRG1 expression by *Lck*-Cre;*Ptpn2*$^{fl/fl}$ CD8⁺ T cells in our earlier experiments was one factor explaining reduced T_{RM} cell numbers in the absence of Ptpn2 expression.

Ptpn2 impacts the transcriptional profile of effector CD8⁺ T cells

Given the important role of Ptpn2 in regulating T cell differentiation in response to chronic systemic infection (LaFleur et al., 2019), we considered that molecular pathways other than KLRG1–ITIM signaling were also involved in restraining the T_{RM} cell potential of Ptpn2-deficient CD8⁺ T cells activated in response to skin infection. To gain more detailed insights into effector differentiation in absence of Ptpn2, we FACS-purified *Lck*-Cre;*Ptpn2*$^{fl/fl}$ and *Ptpn2*$^{fl/fl}$ OT-I cells from spleens of acutely infected mice (as in Fig. 1) and subjected total populations, as well as KLRG1⁻ and KLRG1⁺ subsets, to mRNA sequencing (Fig. 3 A). As expected, we found a large number of differentially expressed genes (DEGs; |log2 (fold change)| >1; false discovery rate <0.05) between KLRG1⁻ and KLRG1⁺ subsets of both *Lck*-Cre; *Ptpn2*$^{fl/fl}$ (712 DEG) and *Ptpn2*$^{fl/fl}$ (528 DEG) OT-I cells. Furthermore, we found 190 DEGs between total populations of Ptpn2-deficient and control OT-I cells (Fig. 3, B and C; and Table S1). Interestingly, genes with differential expression in total *Lck*-Cre; *Ptpn2*$^{fl/fl}$ OT-I cells included those coding for skin-homing and other chemokine receptors, such as *Ccr4*, *Ccr10*, *Ccr7*, and *Cxcr5*, the memory-associated transcription factors *Tcf7* and *Id3*, and genes that form part of transcriptional signatures for T_{RM} cells in various tissues, such as *Xcl1*, *Qpct*, *Itgae* (encoding CD103), *P2rx7*, and *S1pr5* (Mackay et al., 2013; Stark et al., 2018). Gene ontology (GO)–term analysis of DEG (|log2 (fold change)| >0.5) revealed enrichment of pathways associated with cell cycle/division and, conversely, underrepresentation of those associated with immune system processes, signal transduction, and cytokine/chemokine receptor activity in *Lck*-Cre;*Ptpn2*$^{fl/fl}$ relative to *Ptpn2*$^{fl/fl}$ OT-I cells (Figs. S2, S3, and S4). This was consistent with superior early expansion but impaired skin infiltration and T_{RM} cell formation observed for *Lck*-Cre;*Ptpn2*$^{fl/fl}$ OT-I cells in our initial experiments (Fig. 1).

We next asked whether the subpopulations of KLRG1⁻ and KLRG1⁺ cells differed depending on their expression of Ptpn2. Compared with the 190 DEGs for the total effector populations, considerably fewer genes were differentially expressed between *Lck*-Cre;*Ptpn2*$^{fl/fl}$ and *Ptpn2*$^{fl/fl}$ OT-I cells among the KLRG1⁻ (93 DEGs) and KLRG1⁺ (59 DEGs) subsets (Fig. 3, B and C; Table S2; and Table S3). Hierarchical clustering analysis further revealed clustering of KLRG1⁻ cells of both genotypes with total *Ptpn2*$^{fl/fl}$ OT-I cells, whereas KLRG1⁺ cells of both genotypes clustered with total *Lck*-Cre;*Ptpn2*$^{fl/fl}$ OT-I cells (Fig. 3 D), indicating that in vivo–activated Ptpn2-deficient OT-I cells displayed a transcriptional bias toward KLRG1⁺ effectors. Gene set enrichment analysis further showed that differential gene profiles between *Lck*-Cre;*Ptpn2*$^{fl/fl}$ and *Ptpn2*$^{fl/fl}$ OT-I cells for all subfractions (total, KLRG1⁺, and KLRG1⁻) were enriched significantly for previously identified effector versus memory CD8⁺ T cell signature genes (Kaech et al., 2002; Luckey et al., 2006; Fig. 3 E). Taken together, these findings further support the above suggestion that after in vivo priming following HSV infection, Ptpn2 deficiency resulted in the preferential generation of OT-I cells with a transcriptional profile biased toward more terminally differentiated KLRG1⁺ effector cells with restricted memory potential.

Ptpn2-deficient KLRG1⁻ effector cells can form T_{RM} cells

We next compared the capacities of purified KLRG1⁺ and KLRG1⁻ effector cells of both genotypes to form T_{RM} cells. To this end, we isolated and sorted total, KLRG1⁺, and KLRG1⁻ OT-I cells from spleens 8 d after infection and transferred these into new recipient mice infected with HSV-Ova 4 d earlier, followed by analysis of T cell numbers in the skin 30 d after infection (Fig. 4 A). Upon transfer of total effector cells, we recovered 2.2-fold more *Ptpn2*$^{fl/fl}$ than *Lck*-Cre;*Ptpn2*$^{fl/fl}$ OT-I cells from the skin of recipient mice (Fig. 4 B), echoing the differences after transfer of naive OT-I cells (Fig. 1 A). By contrast, purified KLRG1⁻ effector cells generated comparable numbers of total and CD69⁺ CD103⁺ T_{RM} *Ptpn2*$^{fl/fl}$, and *Lck*-Cre;*Ptpn2*$^{fl/fl}$ OT-I cells in skin, whereas purified KLRG1⁺ cells of both genotypes failed to give rise to T_{RM} cells, consistent with previous reports (data not shown; Mackay et al., 2013). Confirming these results, we also found that OT-I cells of both genotypes activated in vitro under conditions that

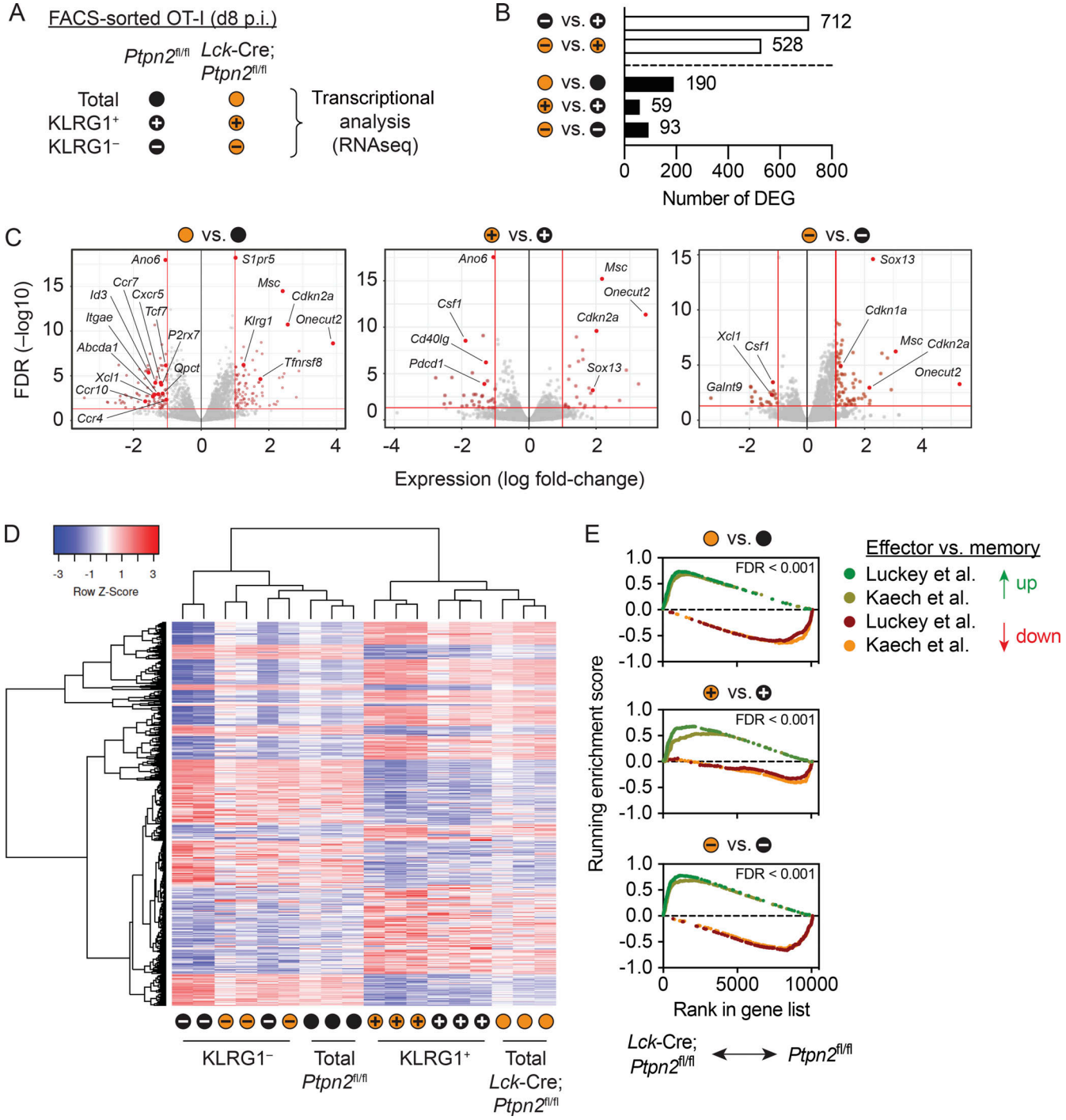

Figure 3. **Ptpn2 regulates the transcriptional profiles of effector CD8⁺ T cells arising after HSV skin infection.** Mice were infected and OT-I cells transferred, as in Fig. 1. Total (empty), KLRG1⁺ (+ symbol), and KLRG1⁻ (– symbol) populations from *Ptpn2*$^{fl/fl}$ (black) and *Lck*-Cre;*Ptpn2*$^{fl/fl}$ (orange) OT-I cells were isolated from spleens 8 d post infection (p.i.), sorted, and subjected to mRNA sequencing. **(A)** List of effector populations and designated symbols used throughout. **(B)** Numbers of differentially regulated genes (DEGs) between various OT-I effector populations, as indicated. **(C)** Volcano plots comparing transcriptional profiles of *Ptpn2*$^{fl/fl}$ and *Lck*-Cre;*Ptpn2*$^{fl/fl}$ OT-I cells for total, KLRG1⁺, and KLRG1⁻ cells populations, as indicated. DEGs are indicated in light red, with selected genes highlighted in dark red. **(D)** Hierarchical clustering of DEG from comparisons in B. **(E)** Gene set enrichment analysis comparing transcriptional profiles between total, KLRG1⁺, and KLRG1⁻ populations of *Ptpn2*$^{fl/fl}$ and *Lck*-Cre;*Ptpn2*$^{fl/fl}$ OT-I cells relative to published datasets comparing effector and memory CD8⁺ T cells (references). Samples derived from *n* = 3 individual experiments with pooled samples from 8–10 donor mice/group. FDR, false discovery rate.

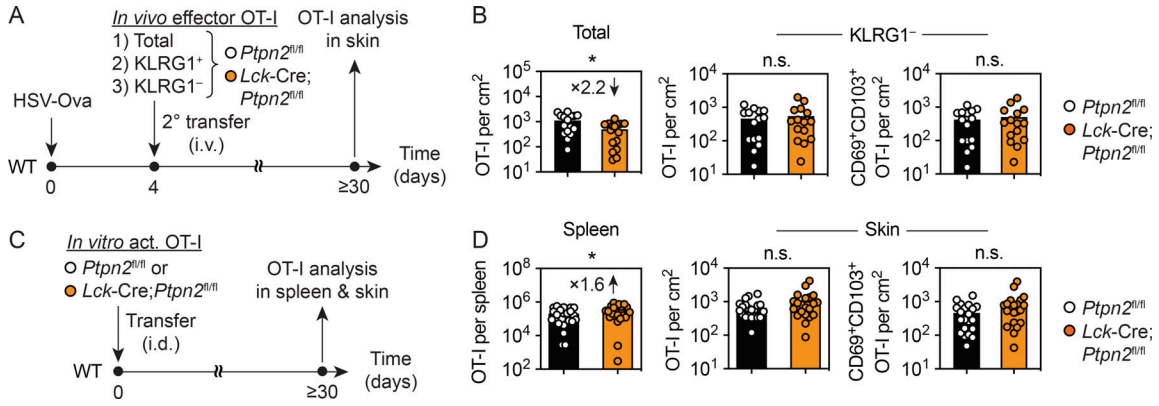

Figure 4. **Absence of Ptpn2 does not impact the ability of KLRG1⁻ effector cells to form T_{RM} cells in skin. (A and B)** Donor mice were infected with HSV-Ova and transferred *Ptpn2*$^{fl/fl}$ (white) or *Lck*-Cre;*Ptpn2*$^{fl/fl}$ (orange) OT-I cells as in Fig. 1. Total (4–10 × 10^4), KLRG1⁺ (1 × 10^4), and KLRG1⁻ (2.5–5 × 10^4) OT-I cells were isolated from spleens 8 d after infection, sorted, and i.v. transferred into congenic mice (2° transfer) infected with HSV-Ova (1 × 10^6 PFU) 4 d earlier. OT-I cells were analyzed in skin ≥30 d after infection. **(B)** Enumeration of total and CD69⁺ CD103⁺ OT-I cells in mice that received total (left) or KLRG1⁻ (middle, right) OT-I cells. Data pooled from *n* = 3 experiments with a total of *n* = 15 mice/group. **(C and D)** *Ptpn2*$^{fl/fl}$ (white) and *Lck*-Cre;*Ptpn2*$^{fl/fl}$ (orange) OT-I cells were activated in vitro and transferred i.d. (5 × 10^6) into congenic recipient mice. OT-I cells in spleen and skin were analyzed ≥30 d later. **(D)** Enumeration of total and CD69⁺ CD103⁺ OT-I cells in spleen (left) and skin (middle, right) of recipient mice. Data pooled from *n* = 5 experiments with a total of *n* = 21 mice/group. Statistical significance (*, P < 0.05) determined by Mann–Whitney test.

do not induce KLRG1 expression generated comparable numbers of T_{RM} cells following direct transfer into the skin by intradermal (i.d.) injection (Fig. 4, C and D). Interestingly, numbers of *Lck*-Cre;*Ptpn2*$^{fl/fl}$ OT-I in spleen were moderately increased compared with *Ptpn2*$^{fl/fl}$ OT-I cells in this setting (Fig. 4 D). Combined, these results revealed that Ptpn2-deficient KLRG1⁻ effector cells have a normal capacity to form T_{RM} cells and further suggested that the defect in T_{RM} cell formation seen in our previous experiments was primarily caused by the relative reduction of KLRG1⁻ cells among the effector pool in spleen and skin (Fig. 1, G–I).

Ptpn2 restrains T_{RM} cell–mediated immunity in the context of skin inflammation and viral infection

Finally, we asked whether Ptpn2 impacted the function of T_{RM} cells in skin. Flow cytometric analysis confirmed sustained Ptpn2 expression by T_{RM} cells generated following skin infection with HSV or by i.d. deposition of in vitro–activated CD8⁺ T cells (Fig. 5 A). The latter approach offered an opportunity to examine the role of Ptpn2 in regulating T_{RM} cell–mediated local immunity. Thus, in a first set of experiments, we generated *Lck*-Cre;*Ptpn2*$^{fl/fl}$ or *Ptpn2*$^{fl/fl}$ OT-I T_{RM} cells in skin of *K5*-rTA;TetO.mOva mice in which expression of membrane-bound Ova (mOva) by skin keratinocytes can be induced following treatment with doxycycline (Dox; Fig. 5 B). Upon induction of Ova, T_{RM} cells in skin are the first to recognize local antigen and precipitate an inflammatory response with appearance of skin lesions focused at sites of highest T_{RM} cell density (Fig. S5 A and data not shown). While the time of disease onset in the first week after Ova induction was comparable between the cohorts harboring *Lck*-Cre;*Ptpn2*$^{fl/fl}$ or *Ptpn2*$^{fl/fl}$ T_{RM} cells, disease progression and overall severity were more pronounced in mice with Ptpn2-deficient OT-I cells (Fig. 5 C). In line with this, *Lck*-Cre;*Ptpn2*$^{fl/fl}$ CD69⁺ CD103⁺ T_{RM} cells produced more granzyme B than their *Ptpn2*$^{fl/fl}$ counterparts at the onset of disease (Figs. 5 D and S5 B). In support of the notion that Ptpn2 fine-tunes T_{RM} cell responses to antigen, separate experiments with WT mice revealed strongly elevated production of granzyme B and IFNγ by *Lck*-Cre;*Ptpn2*$^{fl/fl}$ CD69⁺ CD103⁺ T_{RM} cells in response to low-dose i.d. peptide challenge (Fig. S5 C).

To further refine the role of T_{RM} cells in dermatitis, we generated *Lck*-Cre;*Ptpn2*$^{fl/fl}$ or *Ptpn2*$^{fl/fl}$ OT-I T_{RM} cells in skin of *K5*-rTA;TetO.mOva mice and depleted recirculating CD8⁺ T cells using anti-CD8 depleting antibody, leaving the skin T_{RM} cell population largely intact (Hobbs and Nolz, 2019; data not shown). 9 d later, Ova expression was induced by Dox treatment (Fig. 5 E). As shown in Fig. 5 F, dermatitis developed in the absence of recirculating OT-I cells, confirming that T_{RM} cells were key drivers of disease. Furthermore, dermatitis progression and severity were significantly more pronounced in mice harboring Ptpn2-deficient T_{RM} cells, again emphasizing an important role of Ptpn2 in regulating T_{RM} cell function. Thus, consistent with the established role of Ptpn2 in preventing CD8⁺ T cell–mediated autoimmune disease in models of type I diabetes (Wiede et al., 2019; Wiede et al., 2014b), lack of Ptpn2 expression specifically in T_{RM} cells was sufficient to cause aggravated skin inflammation in a dermatitis model.

In a final set of experiments, we generated *Lck*-Cre;*Ptpn2*$^{fl/fl}$ or *Ptpn2*$^{fl/fl}$ OT-I T_{RM} cells in WT mice by i.d. injection of in vitro activated OT-I T cells and challenged them with HSV-Ova skin infection at the site of initial T_{RM} cell deposition (Fig. 5 G). We have previously shown in related experiments that T_{RM} cells afford a level of rapid protection from HSV challenge infection potent enough to prevent the development of characteristic zosteriform skin lesions (Gebhardt et al., 2009; Mackay et al., 2012). When we measured viral titers in skin harboring Ptpn2-deficient or control T_{RM} cells 4 d after infection, we observed a 100-fold reduction in viral load in skin with Ptpn2-deficient OT-I cells (Fig. 5 H). Combined, these results demonstrate an important role of Ptpn2 beyond the regulation of T cell effector

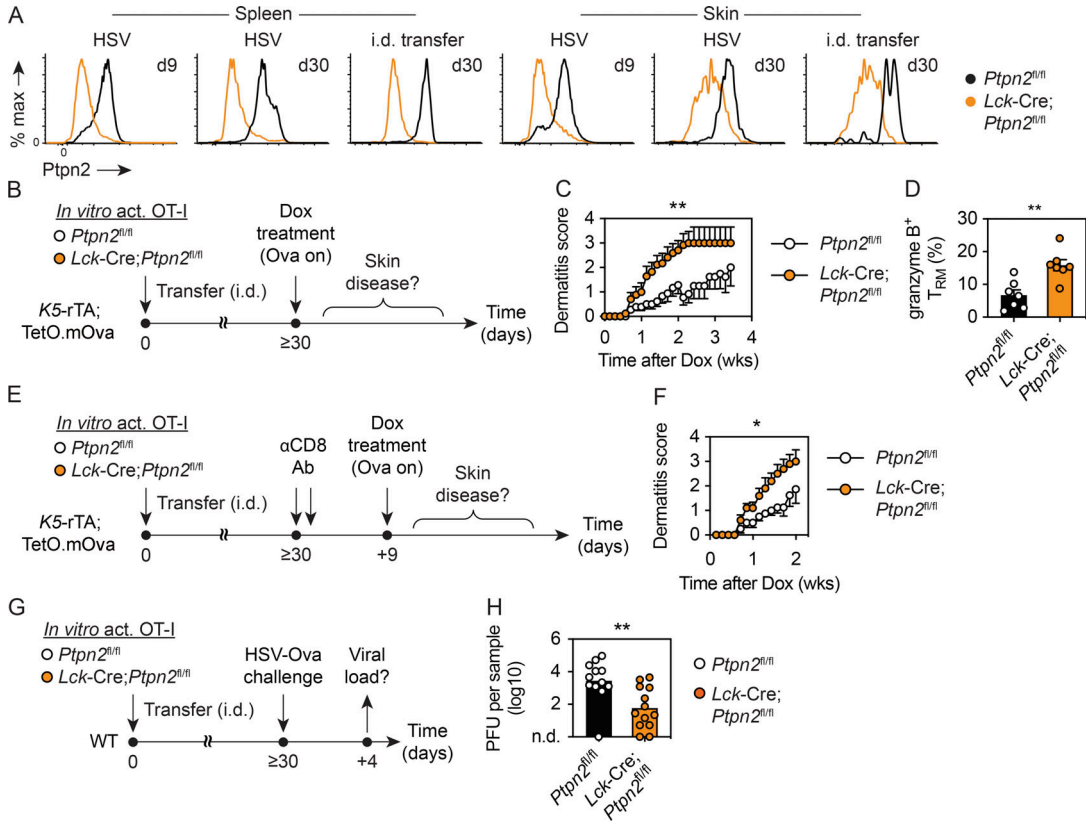

Figure 5. **Ptpn2 regulates T_{RM}-mediated immunity in skin. (A)** Analysis of Ptpn2 expression by *Ptpn2*$^{fl/fl}$ OT-I cells (black) in spleen and skin at indicated times after HSV-Ova infection or i.d. transfer of in vitro activated cells. *Lck*-Cre;*Ptpn2*$^{fl/fl}$ (orange) cells serve as negative control for Ptpn2 staining. **(B–D)** In vitro–activated *Ptpn2*$^{fl/fl}$ and *Lck*-Cre;*Ptpn2*$^{fl/fl}$ OT-I cells were transferred i.d. into *K5*-rTA;TetO.mOva recipients. More than 30 d later, mice were treated with Dox in their drinking water to induce Ova expression, and skin lesions were assessed daily. **(C)** Average dermatitis scores over time for recipients of *Ptpn2*$^{fl/fl}$ (white) and *Lck*-Cre;*Ptpn2*$^{fl/fl}$ (orange) OT-I cells. Mice had received 1–2.5 × 10^6 OT-I cells i.d. >4 wk before Dox treatment; data pooled from *n* = 4 experiments with a total of *n* = 18–22 mice (mean ± SEM). **(D)** Flow cytometric analysis of granzyme B expression by *Ptpn2*$^{fl/fl}$ (white) and *Lck*-Cre;*Ptpn2*$^{fl/fl}$ (orange) T_{RM} cells 5 d after Dox treatment of *K5*-rTA;TetO.mOva recipients. Mice had received 2–5 × 10^6 OT-I cells i.d. >4 wk before Dox treatment; data pooled from *n* = 2 experiments with *n* = 7 mice per group. **(E and F)** In vitro–activated *Ptpn2*$^{fl/fl}$ and *Lck*-Cre;*Ptpn2*$^{fl/fl}$ OT-I cells (2 × 10^6) were transferred i.d. into *K5*-rTA;TetO.mOva recipients. More than 30 d later, circulating CD8$^+$ T cells were depleted by i.p. administration of CD8-depleting antibody (αCD8 Ab; 300 µg and 100 µg) on two consecutive days. 9 d after initial antibody administration, Ova expression was induced as in C and skin lesions assessed daily. **(F)** Average dermatitis scores over time for recipients of *Ptpn2*$^{fl/fl}$ (white) and *Lck*-Cre;*Ptpn2*$^{fl/fl}$ (orange) OT-I cells. Data pooled from *n* = 2 experiments with a total of *n* = 8–10 mice (mean ± SEM). **(G and H)** In vitro activated *Ptpn2*$^{fl/fl}$ and *Lck*-Cre;*Ptpn2*$^{fl/fl}$ OT-I cells (2–5 × 10^6) were transferred i.d. into congenic WT mice, followed by HSV-Ova challenge infection at the site of initial OT-I deposition ≥30 d later. **(H)** Analysis of viral titers in skin 4 d after infection for recipients of *Ptpn2*$^{fl/fl}$ (white) and *Lck*-Cre;*Ptpn2*$^{fl/fl}$ (orange) OT-I cells. Data pooled from *n* = 2 experiments with a total of *n* = 12–13 mice/group. Statistical significance (*, P < 0.05; **, P < 0.01) determined by Mann–Whitney test. For C and D, the area under the curve was calculated for each individual mouse to determine statistical significance.

differentiation; that is, restraining T_{RM} cell–mediated immune responses in the context of skin inflammation and infection.

Discussion

T_{RM} cells are key determinants of effective tissue immunity and as such are promising targets for immunotherapeutic intervention and vaccination in a broad spectrum of diseases, including infection, chronic inflammation, cancer, autoimmunity, and organ transplantation. A detailed understanding of the molecular pathways and environmental factors that regulate their generation, persistence, and function is therefore critical to the rational development of novel immunotherapies aimed at modulating tissue immunity. In the present study, we identified two T cell–intrinsic molecules as new regulators of T_{RM} cell biology in skin; namely, the protein tyrosine phosphatase Ptpn2 and the putatively immunoregulatory receptor, KLRG1.

The function of Ptpn2 in regulating intracellular signaling is critical to the establishment and maintenance of immune tolerance. This is most evident from the observation that genetic deletion of Ptpn2 in immune cells, T cells, or adoptively transferred CD8$^+$ T cells promotes systemic inflammation and autoimmunity, respectively (Wiede et al., 2011; Wiede et al., 2019; Wiede et al., 2014b; Heinonen et al., 2004). Furthermore, single-nucleotide polymorphisms in the human *PTPN2* gene have been linked to development of autoimmunity and chronic inflammatory disorders in patients (Todd et al., 2007; Smyth et al., 2008). Consistent with its molecular function in attenuating TCR and cytokine receptor signaling (Aoki and Matsuda, 2002; Simoncic et al., 2002; ten Hoeve et al., 2002; Wiede et al., 2014a;

Wiede et al., 2011), Ptpn2 has previously been shown to restrain CD8⁺ T cell responses to self-antigen, tumors, and acute and chronic systemic infections, although recirculating memory CD8⁺ T cells can from normally after acute bacterial infection in absence of Ptpn2 (LaFleur et al., 2019; Wiede et al., 2014a; Wiede et al., 2020; Wiede et al., 2011; Wiede et al., 2014b; Flosbach et al., 2020). We describe a similar function of Ptpn2 in regulating effector CD8⁺ T cell differentiation during an acute virus infection of skin. We show that absence of Ptpn2 expression in CD8⁺ T cells results in transient amplification of T cell expansion early after infection, with a strong numerical increase seen predominately for KLRG1⁺ effector cells and an overall transcriptional bias reflecting increased proliferation and decreased memory potential relative to Ptpn2-competent cells. Of note, our results reveal an important consequence of perturbed effector T cell differentiation in the absence of Ptpn2 that is strongly reduced seeding of skin with epidermal-infiltrating KLRG1⁻ memory precursor cells and, consequently, diminished formation of T_{RM} cells at the site of resolved infection. Interestingly, these defects echo transcriptional changes observed already in splenic Ptpn2-deficient T cells before they infiltrate the skin, including down-regulation of genes encoding for skin-targeting chemokine receptors, such as *Ccr4* and *Ccr10*, and perturbed expression of genes associated with T_{RM} cell–specific transcriptional signatures, such as *Xcl1*, *Qpct*, *Itgae*, *P2rx7*, and *S1pr5* (Mackay et al., 2013; Fernandez-Ruiz et al., 2016). Thus, a large fraction of Ptpn2-deficient effector cells in infected skin may be transcriptionally poised in such a way that prohibits commitment to the T_{RM} cell differentiation program. This could also explain their failure to respond appropriately to key environmental cues such as the presence of cognate antigen presented by infected tissue cells (Gebhardt et al., 2009; Khan et al., 2016; Muschaweckh et al., 2016). Furthermore, Ptpn2 deficiency results in a proportional increase in KLRG1⁺ effector cells in skin, and we show that forced expression of KLRG1 alone is sufficient to interfere with T_{RM} cell differentiation.

Expression of KLRG1 identifies terminally differentiated effector CD8⁺ T cells with reduced proliferative capacity and memory potential (Joshi et al., 2007; Sarkar et al., 2008; Voehringer et al., 2001; Voehringer et al., 2002). Nevertheless, its use as memory marker is of limited value in some infections (Croom et al., 2011) and may further be complicated by the more recent demonstration that KLRG1 expression is more dynamic than initially anticipated such that some KLRG1⁺ effector T cells may lose expression of KLRG1 and become long-lived memory cells (Schwartzkopff et al., 2015; Herndler-Brandstetter et al., 2018). Ligation of KLRG1 in vitro has been shown to dampen proliferation and induction of cytolytic function in CD8⁺ T cells (Gründemann et al., 2006). Somewhat surprisingly, however, its genetic deletion has no bearing on splenic memory CD8⁺ T cells generated in response to systemic virus infection (Gründemann et al., 2010). In line with this, we show that forced expression of KLRG1 is inconsequential for the generation of memory T cells in the spleen. Importantly, however, we demonstrate that KLRG1 selectively interferes with the generation of T_{RM} cells in the epidermis, where one of its major ligands, E-cadherin, is expressed constitutively by keratinocytes, Langerhans cells, and T_{RM} cells (Gründemann et al., 2006; Mackay et al., 2013; Hofmann and Pircher, 2011).

KLRG1 shares its ligand E-cadherin with the CD103-incorporating integrin $\alpha_E\beta_7$ (Cepek et al., 1994; Gründemann et al., 2006). Interestingly, expression of all three molecules is regulated by the same T_{RM} cell–instructive cytokine, TGFβ, which induces CD103 and E-cadherin expression in activated CD8⁺ T cells and represses or down-regulates that of KLRG1 (Kilshaw and Murant, 1990; Schwartzkopff et al., 2015; Nath et al., 2019). Of note, T cell–intrinsic CD103 and E-cadherin both support optimal generation and/or maintenance of T_{RM} cells by mediating tethering to neighboring cells and promoting survival and functionality via outside-in signaling (Gebhardt et al., 2018). Binding sites for KLRG1 and $\alpha_E\beta_7$ on E-cadherin are distinct, making sterical hindrance unlikely (Li et al., 2009). However, KLRG1 may exert its inhibitory activity, at least in part, by interfering with signals mediated by CD103 binding to E-cadherin, which may occur either in cis, within the T cells, or in trans, involving interactions of T cells with neighboring epithelial cells. Since KLRG1 expression levels after retroviral transduction were comparable in magnitude with those seen in normal cells responding to virus infection in vivo, it appears unlikely that nonphysiological expression levels caused the observed phenomena. Furthermore, we provide evidence that KLRG1 signaling via its cytoplasmic ITIM contributes to the inhibition of T_{RM} cell formation, which is consistent with previous studies demonstrating that ITIM-mediated signaling can inhibit TCR signaling and T cell proliferation (Beyersdorf et al., 2001; Tessmer et al., 2007; Henson et al., 2009). The signaling-deficient KLRG1-Y7F construct used in our experiments harbors a single point mutation that specifically abrogates ITIM-mediated recruitment of phosphatases (Tessmer et al., 2007; Rosshart et al., 2008), whereas KLRG1–C61-72 has four point mutations that are located to the stalk region crucial for multimerization and therefore prevent multivalent E-cadherin binding and inhibitory signaling (Hofmann et al., 2012). Importantly, both KLRG1 mutants exert weaker inhibitory activity on T_{RM} cell formation, inferring that KLRG1–ITIM signaling hinders T_{RM} cell formation. It should be noted, however, that expression levels of mutant KLRG1 proteins were slightly lower compared with WT KLRG1 and that monomeric KLRG1–C61-72–E-cadherin interactions are of lower affinity (Hofmann et al., 2012). Thus, binding to E-cadherin and putative interference with CD103 signaling may have also been weaker for mutant KLRG1 molecules. Regardless, the combined evidence suggests that repression of KLRG1 is important for normal differentiation of CD69⁺ CD103⁺ T_{RM} cells in skin and further implies that increased expression of KLRG1 seen in Ptpn2-deficient effector cells contributes to their impairment in T_{RM} cell formation.

In chronic infection with lymphocytic choriomeningitis virus, Ptpn2 limits the generation of Tim3⁺ terminally exhausted T cells by preventing excessive type I IFN signaling (LaFleur et al., 2019). It is therefore reasonable to assume that Ptpn2 acts in a similar manner in acute HSV skin infection to restrict JAK-STAT signaling induced by proinflammatory cytokines known to drive terminal differentiation of KLRG1⁺ effector cells,

including type I and II IFN, IL-12, and IL-2 (Kaech and Cui, 2012). Conversely, this implies that under suboptimal or less inflammatory priming conditions, such as during tumor challenge, Ptpn2 deficiency may actually favor the development of memory precursors and T_{RM} cells. In line with this, we and others have recently shown that genetic deletion of Ptpn2 in total T cells, $CD8^+$ T cells or chimeric antigen receptor T cells augments cancer immunity (LaFleur et al., 2019; Wiede et al., 2020). In case of cutaneous melanoma, Ptpn2 deficiency indeed results in enhanced generation of tumor-specific $CD69^+$ $CD103^+$ T_{RM} cells (Wiede et al., 2020), and we have previously shown that these cells can drive long-term melanoma control (Edwards et al., 2018; Hochheiser et al., 2019; Park et al., 2019a). Thus, while Ptpn2 modulates the generation of memory precursor cells in a context-dependent manner, it does not appear to influence the process of T_{RM} cell differentiation in peripheral tissues per se. Our demonstration that in vivo– or in vitro–primed Ptpn2-deficient $KLRG1^-$ effector cells display normal capacities to generate T_{RM} cells upon transfer into new recipients further supports this notion. In these experiments, Ptpn2-deficient $KLRG1^-$ effector cells actually generated more memory T cells in spleen than their WT counterparts, which is in line with a recent report showing superior engraftment after i.v. transfer of briefly in vitro–stimulated $CD8^+$ T cells in absence of Ptpn2 (Flosbach et al., 2020). Both observations may be explained by increased proliferative momentum of activated Ptpn2-deficient cells before transfer, which is also echoed by our combined transcriptional and GO analyses, as well as to their heightened responsiveness to cytokines known to promote the survival and homeostatic turnover of recirculating memory T cells, such as IL-7 and IL-15.

Importantly, we further show that T_{RM} cells maintain expression of Ptpn2 and that its genetic deletion amplifies T_{RM} cell–mediated skin immunity in the context of virus infection and autoantigen-induced inflammation. We speculate that the decreased threshold for productive TCR activation in the absence of Ptpn2 regulation may be the major factor promoting accelerated and possibly augmented effector activity in T_{RM} cells. As such, our results lend strong support to the concept that therapeutic Ptpn2 inhibition may prove beneficial in bolstering protective immunity to fight infection and cancer. At the same time, they corroborate earlier studies in illustrating potential side effects of therapeutic Ptpn2 inhibition; that is, triggering autoimmune inflammation including type I diabetes and dermatitis (Heinonen et al., 2004; Wiede et al., 2019; Wiede et al., 2011; Wiede et al., 2014b). Of note in this respect, our study further emphasizes that T_{RM} cells could be major targets of Ptpn2 inhibition in therapeutic settings. Thus, transient topical application of Ptpn2 inhibitors may prove sufficient to achieve clinical benefit, at least in accessible organs such as skin, which has the added benefit of avoiding potential side effects from systemic dosing. In summary, our study provides fresh insights into the molecular underpinnings of T_{RM} cell generation and function in skin. Future studies will have to explore in more detail the therapeutic implications of our findings for immunomodulatory strategies aimed at modulating T_{RM} cell function in infection and tissue pathology.

Materials and methods

Mice

Female C57BL/6, B6.SJL-PtprcaPep3b/BoyJ (B6.CD45.1), C57BL/6-Tg(*K5*-rTA)04Cbn Tg(TetOmOva)13Cbn/Apb (*K5*-rTA;TetO.mOva), and gBT-I × B6.CD45.1 (gBT-I.CD45.1) mice were bred in the Department of Microbiology and Immunology of The University of Melbourne. *Ptpn2*$^{fl/fl}$;OT-I and *Lck*-Cre;*Ptpn2*$^{fl/fl}$;OT-I are Ptpn2-competent or -deficient mice, respectively, with $CD8^+$ T cells expressing a transgenic T cell receptor specific for the Ova peptide SIINFEKL, as previously described (Wiede et al., 2011), and were bred at the Victorian Comprehensive Cancer Centre. *K5*-rTA;TetO.mOva mice (available from the Australian Phenome Bank) express a Dox-inducible (Tetracycline-on [TetO]) mOva under the control of the keratin 5 (K5) promoter in keratinocytes in the epidermis and hair follicles. In these mice, following oral Dox treatment, rTA expression activates the TetO promoter for mOva expression in the skin. In gBT-I mice, $CD8^+$ T cells express a transgenic T cell receptor recognizing the HSV gB–derived epitope $gB_{498–505}$. All mice were aged between 6 and 12 wk at the start of experimentation, and all experiments were approved by the relevant Animal Ethics Committee of The University of Melbourne.

In vitro activation of transgenic T cells

gBT-I or OT-I splenocytes were activated in vitro by incubation for 4–5 d with gB (SSIEFARL; 0.2 µg/ml; Genescript) or Ova (SIINFEKL; 0.2 µg/ml; Genescript) peptide–pulsed splenocytes in the presence of recombinant human IL-2 (25 U/ml; PeproTech) and lipopolysaccharide (75 ng/ml; Sigma-Aldrich), as previously described (Gebhardt et al., 2009). In some experiments, recombinant human TGFβ1 (10 ng/ml; R&D Systems) was added during the last 2 or 3 d of culture.

Adoptive transfer of $CD8^+$ T cells

Naive *Ptpn2*$^{fl/fl}$ or *Lck*-Cre;*Ptpn2*$^{fl/fl}$ OT-I cells (5×10^4) were transferred i.v. into congenic WT mice infected with HSV-Ova 2 d earlier. In some experiments, total, $KLRG1^+$ or $KLRG1^-$ effector populations ($2.5–10 \times 10^4$) were isolated from spleens of HSV-infected mice, sorted, and transferred i.v. into infected congenic recipients. In vitro–activated OT-I cells were injected i.d. into B6.CD45.1 or *K5*-rTA;TetO.mOva mice ($1–5 \times 10^6$). In other experiments, in vitro–activated and transduced gBT-I cells were i.v. injected into recipient mice ($1–2.5 \times 10^6$) treated on the skin with DNFB, as described previously (Mackay et al., 2012). Genetically modified gBT-I cells derived from bone marrow chimeric mice were transferred i.v. ($2–10 \times 10^4$) into congenic mice infected with HSV-1.

HSV skin infection

HSV-1 skin infection was performed by light skin abrasion using 10^6 PFUs of the KOS strain of HSV-1 or Ova-expressing HSV-1, as described previously (van Lint et al., 2004). Mice were anaesthetized with a mixture of ketamine (100 mg/kg; Parnell Laboratories) and Xylazil (15 mg/kg; Troy Laboratories) by i.p. injection, and lubricating eye gel (Allergen Australia) was applied to the eyes to prevent drying. Mice were shaved with a razor (Wahl) and depilated using Veet cream (Reckitt Benckiser)

before skin was lightly abraded with a power tool (Dremel) and 10 µl virus solution applied to abraded skin. An adhesive waterproof film (Opsite) was used to cover the virus, and mice were bandaged with micropore and macropore tape for 2 d. For HSV challenge experiments, virus titers in skin were determined by removing and homogenizing a 1-cm^2 area of skin that was assayed for infectious virus by plaque assay on Vero cells (CSL Australia), as described previously (van Lint et al., 2004).

Treatment with DNFB

Mice were anaesthetized with ketamine (100 mg/kg; Parnell Laboratories) and Xylazil (15 mg/kg; Troy Laboratories) by i.p. injection. Skin was shaved and depilated before 15 µl of DNFB (0.25%) in acetone and oil (4:1 vol/vol) was applied to a 1.5cm^2 area of flank skin.

Dermatitis model

In vitro–activated OT-I cells were transferred i.d. into *K5*-rTA; TetO.mOva mice. More than 4 wk later, circulating CD8-expressing cells were depleted in cohorts of mice by i.p. administration of 300 µg and 100 µg CD8-depleting antibody (clone 2.43; Walter and Eliza Hall Institute), respectively, on two consecutive days. Absence of circulating $CD8^+$ T cells in the blood was confirmed 5 d later by flow cytometry. Starting 9 d after CD8 depletion, mice were continuously treated with Dox in their drinking water (1 mg/ml). To assess skin inflammation, mice were shaved and depilated using Veet cream. Dermatitis was quantified using the following scoring system (from 0 to 4): 0, no signs of disease; 1, marginally dry or red skin; 2, early developing lesions covering <10% of flanks; 3, developed lesions, covering >10% and <50% of flanks; 4, pronounced lesions covering >50% of the flank. Mice were euthanized when reaching a score of 4 but were kept in the analysis with score 4 until the end of the experiment to calculate the area under the curve for statistical evaluation.

In vivo peptide challenge

In vitro–activated OT-I cells were transferred i.d. into WT mice. More than 4 wk later, mice were shaved and depilated using Veet cream, and 0.1 µg Ova peptide SIINFEKL (Genescript) was i.d. injected in a volume of 100 µl PBS. Skin was harvested 6 h later, and cells were isolated in the presence of 10 µg/ml Brefeldin A (Sigma-Aldrich).

Flow cytometry and antibodies

Mice were perfused with 10 ml PBS (Media Preparation Unit, University of Melbourne) before tissues were harvested. Lymphocytes were isolated from the spleen by grinding organs through a metal mesh to create single-cell suspensions. T cells were isolated from the skin as described previously (Gebhardt et al., 2009; Mackay et al., 2013). Briefly, skin was incubated in dispase solution (2.5 mg/ml; Roche) for 90 min and the epidermis separated from the dermis. The dermis was finely chopped and incubated in collagenase type III (3 mg/ml; Worthington) and the epidermis placed in trypsin (0.25%) and EDTA (0.1%, in PBS; Sigma-Aldrich) and incubated for 30 min at 37°C. Samples were filtered through a 75-µm mesh, and single-cell suspensions were stained with antibodies for flow cytometry. For cell sorting, $CD8^+$ T cells were enriched from the spleen by incubation with anti-CD4 (GK1.5), anti-Mac-1α (clone M1/70), anti-F4/80 (clone F4/80), anti-erythrocyte (clone TER-119), and anti-I-A/E (clone M5114) monoclonal antibodies, followed by incubation with goat anti-rat IgG-coupled magnetic beads and removal of bead-bound cells. Isolated cells were surface-stained with the following antibodies: anti-mouse CD8a-FITC/APC/PE (53–6.7; BD Biosciences), CD8β-Alexa Fluor 700 (YTS156.77; BioLegend), CD45.2-AF780/BV786 (104; eBioscience or BD Biosciences), Vα2-PeCy7/BV421 (B20.1; BD Biosciences), Vβ5.1/5.2-PE (9MR9-4, BioLegend), CD69-PE/APC (H1.2F3; eBioscience), CD16/CD32 (2.4G2; BD Biosciences), CD45.1-AF700/AF780 (A20; BD Biosciences or eBioscience), CD103-FITC (2E7; eBioscience), CD103-APC/PerCPCy5.5 (2E7; BioLegend), KLRG1-FITC/APC/BV605 (2F1; eBioscience or BioLegend), and CD127-APC (A7R34; eBioscience). Cell viability was determined using a fixable LIVE/DEAD near-infrared cell-staining kit (BD Biosciences), propidium iodide (Sigma-Aldrich), or DAPI (BioLegend). SPHERO calibration particles (BD PharMingen) were used for cell enumeration. For intracellular cytokine staining, surface-stained cells were fixed and permeabilized with BD Cytofix/Cytoperm (BD Biosciences) for 20 min on ice, and subsequent washing and staining steps were performed using Perm/Wash Buffer (BD Bioscience). Intracellular staining was performed overnight at 4°C using the antibodies IFNγ-FITC/PECy7 (XMG1.2; BD PharMingen) and granzyme B-PECy7 (NGZB; eBioscience). For staining of Ptpn2, surface-stained cells were fixed in 2% paraformaldehyde for 15 min at room temperature, washed with PBS, and permeabilized with ice-cold methanol/acetone (50:50 vol/vol) for 30 min on ice. Cells were washed three times with 5% FCS in PBS and stained with mouse anti-Ptpn2 (6F3; Medimabs) for 1 h at room temperature. Subsequently, cells were washed three times with 5% FCS in PBS and stained with anti-mouse IgG H+L F(ab)2 fragment–Alexa Fluor 647 (Molecular Probes, Invitrogen) for 30 min at room temperature and washed three times with 5% FCS in PBS before analysis. Cells were sorted using a BD FACS Aria III or analyzed using a BD FACS Canto II or BD Fortessa. Data were analyzed using FlowJo version 9 or 10.

Immunofluorescence microscopy

Skin was harvested into 20% sucrose (Sigma-Aldrich) in PBS for 30 min on ice and snap frozen in tissue-tek OCT compound (Sakura Finetek) with liquid nitrogen. Samples were cut into 20-µm thin slices using a microtome (Leica) and placed on charged glass slides. Samples were air-dried for at least 2 h and then rehydrated with PBS for 5 min. Protein block (DAKO) was applied for 30 min at room temperature in a semihumidified chamber. Sections were stained with Alexa Fluor 647–conjugated CD45.2 (clone A20; BioLegend) for 45 min and then washed four times for 3 min with PBS. Hoechst 33342 (Bio-Rad) was added for 3 min to visualize cell nuclei and then washed off with PBS before mounting. Tiled images were acquired with a Zeiss LSM780 confocal microscope at 20× zoom and processed with Imaris8 (Bitplane) software. Cells in skin epithelium (epidermis and hair follicle epithelium) and dermis were manually

counted in two sections per mouse, and the ratio of cells was calculated for each individual mouse.

Transcriptional analysis by mRNA sequencing

RNA was extracted from sorted in vivo primed effector OT-I using TRIzol reagent (Invitrogen) and Direct-zol RNA MiniPrep columns (Zymo) as described previously (Russ et al., 2014). RNA quality was confirmed using a Bioanalyser, and paired-end libraries were prepared for mRNA-seq using an Illumina TruSeq RNA v2 kit and sequenced using an Illumina HiSeq2500. Reads where aligned to mm10 genome using TopHat, reads were assigned to genes using Subread R package, and differential expression was performed using edgeR R package. Genes were deemed differentially expressed if the adjusted P value was < 0.05 and |log2 (fold change)| > 1. For GO-term analysis, genes with false discovery rate < 0.05 and |log2 (fold change)| > 0.5 were taken into account. Genes with read counts of <5 were removed from the analysis. Data were visualized using RStudio (integrated development for R; RStudio). The GEO accession number for submitted RNA-sequencing data is GSE166133. Gene set enrichment analysis (Mootha et al., 2003, Subramanian et al., 2005) was performed with the following gene sets from the molecular signatures database (MSigDB) 3.0 (Liberzon et al., 2011): KAECH_DAY8_EFF_VS_MEMORY_CD8_TCELL_DN/UP (Kaech et al., 2002) and GOLDRATH_EFF_VS_MEMORY_CD8_TCELL_DN/UP (Luckey et al., 2006).

Retroviral constructs

Vectors encoding murine *Klrg1.WT* (NCBI reference sequence NM_016970.1), *Klrg1*.Y7F (TAT → TTT) and *Klrg1*.C61-72 (C61S TGC → AGC, C62Q TGC → CAA, C69S TGT → TCT, C72S TGC → AGC) cDNA flanked by Bgl2 and Mfe1 restriction sites were ordered from Integrated DNA Technologies IDT. Gene fragments were removed from IDT vectors using Bgl2 (New England Biolabs) and MfeI (New England Biolabs) digestion and inserted into the multiple cloning site of the murine stem cell virus/internal ribosome entry site GFP vector (pMIG, plasmid 9044; Addgene), linearized with Bgl2 (New England Biolabs) and EcoR1 (New England Biolabs).

Production of viral particles and transduction of CD8⁺ T cells and bone marrow cells

Viral particles were produced in 293T human embryonic kidney cells with 10 µg vector DNA along with the packaging retroviral constructs GAG (4.8 µg) and pEco (2.4 µg) using standard calcium phosphate precipitation. Supernatant was collected at 48 h, passed through a 0.45-µm filter, and spun onto non–tissue culture–treated 12-well plates (In Vitro Technologies) coated overnight with 32 µg/ml retronectin (Takara) at 3,000 r.p.m and 32°C for 90 min. Supernatant was removed, and 10^6 CD8⁺ T cells were incubated overnight on virus-coated plates in the presence of recombinant human IL-2 (25 U/ml; PeproTech), starting 2 d after in vitro activation with peptide-pulsed splenocytes. Alternatively, bone marrow cells from gBT-I.CD45.1 mice (isolated 1 d prior) were cultured overnight on virus-coated plates in the presence of stem cell factor (100 ng/ml), IL-6 (10 ng/ml), thrombopoietin (50 ng/ml; Shenandoah Biotechnology), and FLt3L (10 ng/ml; BioXCell). Transduction efficiency was determined by GFP expression.

Generation of bone marrow chimeric mice

C57BL/6 mice were lethally irradiated (2 × 550 rad, 3 h apart), i.v. transferred with retrovirally transduced bone marrow cells ($1–4 \times 10^6$), and allowed to reconstitute for at least 8 wk.

Statistical analysis

Data were analyzed and plotted using Prism 8 (GraphPad Software). Comparisons between two groups were performed using a two-tailed Mann–Whitney test, unless indicated otherwise. Differences between groups were considered significant for P values of <0.05.

Online supplemental material

Fig. S1 shows CD103 expression by in vitro–activated T cells in response to TGFβ (*Ptpn2*$^{fl/fl}$ versus *Lck*-Cre;*Ptpn2*$^{fl/fl}$ and pMIG.*Klrg1*.WT versus pMIG.Ctrl), numbers of CD103⁺ OT-I cells in epidermis and dermis in both flanks of mice infected with HSV-Ova and HSV-WT, and mean numbers of KLRG1⁻ *Ptpn2*$^{fl/fl}$ and *Lck*-Cre;*Ptpn2*$^{fl/fl}$ cells in spleen and skin. Fig. S2 lists significantly (P < 0.05) regulated biological processes (GO-term analysis) comparing transcriptional profiles of total, KLRG1⁺, and KLRG1⁻ populations from *Ptpn2*$^{fl/fl}$ and *Lck*-Cre;*Ptpn2*$^{fl/fl}$ OT-I cells, as in Fig. 3. Fig. S3 lists significantly (P < 0.05) regulated cellular components (GO-term analysis) comparing transcriptional profiles of total, KLRG1⁺, and KLRG1⁻ populations from *Ptpn2*$^{fl/fl}$ and *Lck*-Cre;*Ptpn2*$^{fl/fl}$ OT-I cells, as in Fig. 3. Fig. S4 lists significantly (P < 0.05) regulated molecular functions (GO-term analysis) comparing transcriptional profiles of total, KLRG1⁺, and KLRG1⁻ populations from *Ptpn2*$^{fl/fl}$ and *Lck*-Cre;*Ptpn2*$^{fl/fl}$ OT-I cells, as in Fig. 3. Fig. S5 shows representative images of Dox-treated *K5*-rTA;TetO.mOva mice with *Ptpn2*$^{fl/fl}$ and *Lck*-Cre;*Ptpn2*$^{fl/fl}$ T_{RM} cells and granzyme B and cytokine production by *Ptpn2*$^{fl/fl}$ and *Lck*-Cre;*Ptpn2*$^{fl/fl}$ T_{RM} cell after Dox treatment or specific peptide challenge, respectively. Table S1, Table S2, and Table S3 list DEGs between *Ptpn2*$^{fl/fl}$ and *Lck*-Cre;*Ptpn2*$^{fl/fl}$ OT-I cells for total, KLRG1⁺, and KLRG1⁻ populations, respectively.

Acknowledgments

We thank the Flow Cytometry Core Facility, the Melbourne Bioresource Facility, and the Biological Optical Microscopy Platform at the University of Melbourne for technical support.

This study was supported by the National Health and Medical Research Council of Australia (grant APP1084805 to T. Gebhardt; grant APP1059514 to T. Gebhardt, D. Tscharke, and S. Bedoui; and grant APP1184615 to T. Tiganis). K. Hochheiser was supported by the German Research Council (grant HO 5417/1-1) and is a Rhian and Paul Brazis Fellow in Translational Melanoma Immunology administered by the Peter MacCallum Cancer Foundation. T. Gebhardt is a Senior Biomedical Research Fellow supported by the Sylvia and Charles Viertel Charitable Foundation. T. Tiganis is a National Health and Medical Research Council of Australia Principal Research Fellow (APP1103037). S.L. Park was supported by an Elizabeth & Vernon Puzey

postgraduate scholarship and a Cancer Council Victoria postdoctoral fellowship. M.J. Herold is supported by the National Health and Medical Research Council of Australia (grants APP1186575, APP1159658, and APP1156095) and the Leukemia and Lymphoma Society (grant LLS SCOR 7001-13).

Author contributions: Conceptualization: K. Hochheiser, F. Wiede, T. Tiganis, S. Bedoui, and T. Gebhardt; Data curation: K. Hochheiser, B. Russ, C.M. Jones, and T. Gebhardt; Formal analysis: K. Hochheiser, M.H. Enders, M. Olshansky, B. Russ, T. Tiganis, and T. Gebhardt; Funding acquisition: K. Hochheiser, T. Tiganis, S. Bedoui, and T. Gebhardt; Investigation: K. Hochheiser, T. Wagner, D. Freestone, M.H. Enders, B. Russ, S. Nüssing, E. Bawden, Asolina Braun, Annabell Bachem, E. Gressier, R. McConville, S.L. Park, C.M. Jones, and S. Turner; Methodology: F. Wiede, C.M. Jones, G.M. Davey, I.A. Parish, and M.J. Herold; Project administration: K. Hochheiser, S. Bedoui, and T. Gebhardt; Resources: F. Wiede, C.M. Jones, G.M. Davey, D. Tscharke, S. Turner, and T. Tiganis; Software: M. Olshansky; Supervision: D.E. Gyorki, I.A. Parish, T. Tiganis, S. Bedoui, and T. Gebhardt; Validation: K. Hochheiser, T. Wagner, and T. Gebhardt; Visualization: K. Hochheiser, M.H. Enders, D.E. Gyorki, and T. Gebhardt; Writing – original draft: K. Hochheiser, C.M. Jones, and T. Gebhardt; Writing – review & editing: K. Hochheiser, F. Wiede, S.L. Park, G.M. Davey, D.E. Gyorki, I.A. Parish, S. Turner, T. Tiganis, S. Bedoui, and T. Gebhardt.

Disclosures: The authors declare no competing interests exist.

Submitted: 8 May 2020
Revised: 21 December 2020
Accepted: 10 February 2021

References

Aoki, N., and T. Matsuda. 2002. A nuclear protein tyrosine phosphatase TC-PTP is a potential negative regulator of the PRL-mediated signaling pathway: dephosphorylation and deactivation of signal transducer and activator of transcription 5a and 5b by TC-PTP in nucleus. *Mol. Endocrinol.* 16:58–69. https://doi.org/10.1210/mend.16.1.0761

Beyersdorf, N.B., X. Ding, K. Karp, and T. Hanke. 2001. Expression of inhibitory "killer cell lectin-like receptor G1" identifies unique subpopulations of effector and memory CD8 T cells. *Eur. J. Immunol.* 31: 3443–3452. https://doi.org/10.1002/1521-4141(200112)31:12<3443::AID-IMMU3443>3.0.CO;2-J

Casey, K.A., K.A. Fraser, J.M. Schenkel, A. Moran, M.C. Abt, L.K. Beura, P.J. Lucas, D. Artis, E.J. Wherry, K. Hogquist, et al. 2012. Antigen-independent differentiation and maintenance of effector-like resident memory T cells in tissues. *J. Immunol.* 188:4866–4875. https://doi.org/10.4049/jimmunol.1200402

Cepek, K.L., S.K. Shaw, C.M. Parker, G.J. Russell, J.S. Morrow, D.L. Rimm, and M.B. Brenner. 1994. Adhesion between epithelial cells and T lymphocytes mediated by E-cadherin and the alpha E beta 7 integrin. *Nature.* 372:190–193. https://doi.org/10.1038/372190a0

Clark, R.A. 2015. Resident memory T cells in human health and disease. *Sci. Transl. Med.* 7:269rv1. https://doi.org/10.1126/scitranslmed.3010641

Croom, H.A., A.E. Denton, S.A. Valkenburg, N.G. Swan, M.R. Olson, S.J. Turner, P.C. Doherty, and K. Kedzierska. 2011. Memory precursor phenotype of CD8+ T cells reflects early antigenic experience rather than memory numbers in a model of localized acute influenza infection. *Eur. J. Immunol.* 41:682–693. https://doi.org/10.1002/eji.201040625

Edwards, J., J.S. Wilmott, J. Madore, T.N. Gide, C. Quek, A. Tasker, A. Ferguson, J. Chen, R. Hewavisenti, P. Hersey, et al. 2018. CD103+ tumor-resident CD8+ T cells are associated with improved survival in immunotherapy naive melanoma patients and expand significantly during anti-PD1 treatment. *Clin. Cancer Res.* 24:3036–3045. https://doi.org/10.1158/1078-0432.CCR-17-2257

Fernandez-Ruiz, D., W.Y. Ng, L.E. Holz, J.Z. Ma, A. Zaid, Y.C. Wong, L.S. Lau, V. Mollard, A. Cozijnsen, N. Collins, et al. 2016. Liver-Resident Memory CD8$^+$ T Cells Form a Front-Line Defense against Malaria Liver-Stage Infection. *Immunity.* 45:889–902. https://doi.org/10.1016/j.immuni.2016.08.011

Flosbach, M., S.G. Oberle, S. Scherer, J. Zecha, M. von Hoesslin, F. Wiede, V. Chennupati, J.G. Cullen, M. List, J.K. Pauling, et al. 2020. PTPN2 Deficiency Enhances Programmed T Cell Expansion and Survival Capacity of Activated T Cells. *Cell Rep.* 32:107957. https://doi.org/10.1016/j.celrep.2020.107957

Gebhardt, T., L.M. Wakim, L. Eidsmo, P.C. Reading, W.R. Heath, and F.R. Carbone. 2009. Memory T cells in nonlymphoid tissue that provide enhanced local immunity during infection with herpes simplex virus. *Nat. Immunol.* 10:524–530. https://doi.org/10.1038/ni.1718

Gebhardt, T., U. Palendira, D.C. Tscharke, and S. Bedoui. 2018. Tissue-resident memory T cells in tissue homeostasis, persistent infection, and cancer surveillance. *Immunol. Rev.* 283:54–76. https://doi.org/10.1111/imr.12650

Gründemann, C., M. Bauer, O. Schweier, N. von Oppen, U. Lässing, P. Saudan, K.F. Becker, K. Karp, T. Hanke, M.F. Bachmann, and H. Pircher. 2006. Cutting edge: identification of E-cadherin as a ligand for the murine killer cell lectin-like receptor G1. *J. Immunol.* 176:1311–1315. https://doi.org/10.4049/jimmunol.176.3.1311

Gründemann, C., S. Schwartzkopff, M. Koschella, O. Schweier, C. Peters, D. Voehringer, and H. Pircher. 2010. The NK receptor KLRG1 is dispensable for virus-induced NK and CD8+ T-cell differentiation and function in vivo. *Eur. J. Immunol.* 40:1303–1314. https://doi.org/10.1002/eji.200939771

Heinonen, K.M., F.P. Nestel, E.W. Newell, G. Charette, T.A. Seemayer, M.L. Tremblay, and W.S. Lapp. 2004. T-cell protein tyrosine phosphatase deletion results in progressive systemic inflammatory disease. *Blood.* 103:3457–3464. https://doi.org/10.1182/blood-2003-09-3153

Henson, S.M., O. Franzese, R. Macaulay, V. Libri, R.I. Azevedo, S. Kiani-Alikhan, F.J. Plunkett, J.E. Masters, S. Jackson, S.J. Griffiths, et al. 2009. KLRG1 signaling induces defective Akt (ser473) phosphorylation and proliferative dysfunction of highly differentiated CD8+ T cells. *Blood.* 113:6619–6628. https://doi.org/10.1182/blood-2009-01-199588

Herndler-Brandstetter, D., H. Ishigame, R. Shinnakasu, V. Plajer, C. Stecher, J. Zhao, M. Lietzenmayer, L. Kroehling, A. Takumi, K. Kometani, et al. 2018. KLRG1$^+$ Effector CD8$^+$ T Cells Lose KLRG1, Differentiate into All Memory T Cell Lineages, and Convey Enhanced Protective Immunity. *Immunity.* 48:716–729.e8. https://doi.org/10.1016/j.immuni.2018.03.015

Hobbs, S.J., and J.C. Nolz. 2019. Targeted Expansion of Tissue-Resident CD8$^+$ T Cells to Boost Cellular Immunity in the Skin. *Cell Rep.* 29: 2990–2997.e2. https://doi.org/10.1016/j.celrep.2019.10.126

Hochheiser, K., H.X. Aw Yeang, T. Wagner, C. Tutuka, A. Behren, J. Waithman, C. Angel, P.J. Neeson, T. Gebhardt, and D.E. Gyorki. 2019. Accumulation of CD103$^+$ CD8$^+$ T cells in a cutaneous melanoma micrometastasis. *Clin. Transl. Immunology.* 8:e1100. https://doi.org/10.1002/cti2.1100

Hofmann, M., and H. Pircher. 2011. E-cadherin promotes accumulation of a unique memory CD8 T-cell population in murine salivary glands. *Proc. Natl. Acad. Sci. USA.* 108:16741–16746. https://doi.org/10.1073/pnas.1107200108

Hofmann, M., O. Schweier, and H. Pircher. 2012. Different inhibitory capacities of human and mouse KLRG1 are linked to distinct disulfide-mediated oligomerizations. *Eur. J. Immunol.* 42:2484–2490. https://doi.org/10.1002/eji.201142357

Joshi, N.S., W. Cui, A. Chandele, H.K. Lee, D.R. Urso, J. Hagman, L. Gapin, and S.M. Kaech. 2007. Inflammation directs memory precursor and short-lived effector CD8(+) T cell fates via the graded expression of T-bet transcription factor. *Immunity.* 27:281–295. https://doi.org/10.1016/j.immuni.2007.07.010

Kaech, S.M., and W. Cui. 2012. Transcriptional control of effector and memory CD8+ T cell differentiation. *Nat. Rev. Immunol.* 12:749–761. https://doi.org/10.1038/nri3307

Kaech, S.M., S. Hemby, E. Kersh, and R. Ahmed. 2002. Molecular and functional profiling of memory CD8 T cell differentiation. *Cell.* 111: 837–851. https://doi.org/10.1016/S0092-8674(02)01139-X

Khan, T.N., J.L. Mooster, A.M. Kilgore, J.F. Osborn, and J.C. Nolz. 2016. Local antigen in nonlymphoid tissue promotes resident memory CD8+ T cell formation during viral infection. *J. Exp. Med.* 213:951–966. https://doi.org/10.1084/jem.20151855

Kilshaw, P.J., and S.J. Murant. 1990. A new surface antigen on intraepithelial lymphocytes in the intestine. *Eur. J. Immunol.* 20:2201–2207. https://doi.org/10.1002/eji.1830201008

LaFleur, M.W., T.H. Nguyen, M.A. Coxe, B.C. Miller, K.B. Yates, J.E. Gillis, D.R. Sen, E.F. Gaudiano, R. Al Abosy, G.J. Freeman, et al. 2019. PTPN2 regulates the generation of exhausted CD8$^+$ T cell subpopulations and restrains tumor immunity. *Nat. Immunol.* 20:1335–1347. https://doi.org/10.1038/s41590-019-0480-4

Li, Y., M. Hofmann, Q. Wang, L. Teng, L.K. Chlewicki, H. Pircher, and R.A. Mariuzza. 2009. Structure of natural killer cell receptor KLRG1 bound to E-cadherin reveals basis for MHC-independent missing self recognition. *Immunity.* 31:35–46. https://doi.org/10.1016/j.immuni.2009.04.019

Liberzon, A., A. Subramanian, R. Pinchback, H. Thorvaldsdóttir, P. Tamayo, and J.P. Mesirov. 2011. Molecular signatures database (MSigDB) 3.0. *Bioinformatics.* 27:1739–1740. https://doi.org/10.1093/bioinformatics/btr260

Luckey, C.J., D. Bhattacharya, A.W. Goldrath, I.L. Weissman, C. Benoist, and D. Mathis. 2006. Memory T and memory B cells share a transcriptional program of self-renewal with long-term hematopoietic stem cells. *Proc. Natl. Acad. Sci. USA.* 103:3304–3309. https://doi.org/10.1073/pnas.0511137103

Mackay, L.K., A.T. Stock, J.Z. Ma, C.M. Jones, S.J. Kent, S.N. Mueller, W.R. Heath, F.R. Carbone, and T. Gebhardt. 2012. Long-lived epithelial immunity by tissue-resident memory T (TRM) cells in the absence of persisting local antigen presentation. *Proc. Natl. Acad. Sci. USA.* 109:7037–7042. https://doi.org/10.1073/pnas.1202288109

Mackay, L.K., A. Rahimpour, J.Z. Ma, N. Collins, A.T. Stock, M.L. Hafon, J. Vega-Ramos, P. Lauzurica, S.N. Mueller, T. Stefanovic, et al. 2013. The developmental pathway for CD103(+)CD8+ tissue-resident memory T cells of skin. *Nat. Immunol.* 14:1294–1301. https://doi.org/10.1038/ni.2744

Mackay, L.K., M. Minnich, N.A. Kragten, Y. Liao, B. Nota, C. Seillet, A. Zaid, K. Man, S. Preston, D. Freestone, et al. 2016. Hobit and Blimp1 instruct a universal transcriptional program of tissue residency in lymphocytes. *Science.* 352:459–463. https://doi.org/10.1126/science.aad2035

Mootha, V.K., C.M. Lindgren, K.F. Eriksson, A. Subramanian, S. Sihag, J. Lehar, P. Puigserver, E. Carlsson, M. Ridderstråle, E. Laurila, et al. 2003. PGC-1alpha-responsive genes involved in oxidative phosphorylation are coordinately downregulated in human diabetes. *Nat. Genet.* 34:267–273. https://doi.org/10.1038/ng1180

Muschaweckh, A., V.R. Buchholz, A. Fellenzer, C. Hessel, P.A. König, S. Tao, R. Tao, M. Heikenwälder, D.H. Busch, T. Korn, et al. 2016. Antigen-dependent competition shapes the local repertoire of tissue-resident memory CD8+ T cells. *J. Exp. Med.* 213:3075–3086. https://doi.org/10.1084/jem.20160888

Nath, A.P., A. Braun, S.C. Ritchie, F.R. Carbone, L.K. Mackay, T. Gebhardt, and M. Inouye. 2019. Comparative analysis reveals a role for TGF-β in shaping the residency-related transcriptional signature in tissue-resident memory CD8+ T cells. *PLoS One.* 14:e0210495. https://doi.org/10.1371/journal.pone.0210495

Park, C.O., and T.S. Kupper. 2015. The emerging role of resident memory T cells in protective immunity and inflammatory disease. *Nat. Med.* 21:688–697. https://doi.org/10.1038/nm.3883

Park, S.L., A. Buzzai, J. Rautela, J.L. Hor, K. Hochheiser, M. Effern, N. McBain, T. Wagner, J. Edwards, R. McConville, et al. 2019a. Tissue-resident memory CD8$^+$ T cells promote melanoma-immune equilibrium in skin. *Nature.* 565:366–371. https://doi.org/10.1038/s41586-018-0812-9

Park, S.L., T. Gebhardt, and L.K. Mackay. 2019b. Tissue-Resident Memory T Cells in Cancer Immunosurveillance. *Trends Immunol.* 40:735–747. https://doi.org/10.1016/j.it.2019.06.002

Rosshart, S., M. Hofmann, O. Schweier, A.K. Pfaff, K. Yoshimoto, T. Takeuchi, E. Molnar, W.W. Schamel, and H. Pircher. 2008. Interaction of KLRG1 with E-cadherin: new functional and structural insights. *Eur. J. Immunol.* 38:3354–3364. https://doi.org/10.1002/eji.200838690

Russ, B.E., M. Olshanksy, H.S. Smallwood, J. Li, A.E. Denton, J.E. Prier, A.T. Stock, H.A. Croom, J.G. Cullen, M.L. Nguyen, et al. 2014. Distinct epigenetic signatures delineate transcriptional programs during virus-specific CD8(+) T cell differentiation. *Immunity.* 41:853–865. https://doi.org/10.1016/j.immuni.2014.11.001

Sarkar, S., V. Kalia, W.N. Haining, B.T. Konieczny, S. Subramaniam, and R. Ahmed. 2008. Functional and genomic profiling of effector CD8 T cell subsets with distinct memory fates. *J. Exp. Med.* 205:625–640. https://doi.org/10.1084/jem.20071641

Sathaliyawala, T., M. Kubota, N. Yudanin, D. Turner, P. Camp, J.J. Thome, K.L. Bickham, H. Lerner, M. Goldstein, M. Sykes, et al. 2012. Distribution and compartmentalization of human circulating and tissue-resident memory T cell subsets. *Immunity.* 38:187–197. https://doi.org/10.1016/j.immuni.2012.09.020

Schwartzkopff, S., S. Woyciechowski, U. Aichele, T. Flecken, N. Zhang, R. Thimme, and H. Pircher. 2015. TGF-β downregulates KLRG1 expression in mouse and human CD8(+) T cells. *Eur. J. Immunol.* 45:2212–2217. https://doi.org/10.1002/eji.201545634

Sheridan, B.S., Q.M. Pham, Y.T. Lee, L.S. Cauley, L. Puddington, and L. Lefrançois. 2014. Oral infection drives a distinct population of intestinal resident memory CD8(+) T cells with enhanced protective function. *Immunity.* 40:747–757. https://doi.org/10.1016/j.immuni.2014.03.007

Simoncic, P.D., A. Lee-Loy, D.L. Barber, M.L. Tremblay, and C.J. McGlade. 2002. The T cell protein tyrosine phosphatase is a negative regulator of janus family kinases 1 and 3. *Curr. Biol.* 12:446–453. https://doi.org/10.1016/S0960-9822(02)00697-8

Smazynski, J., and J.R. Webb. 2018. Resident Memory-Like Tumor-Infiltrating Lymphocytes (TIL$_{RM}$): Latest Players in the Immuno-Oncology Repertoire. *Front. Immunol.* 9:1741. https://doi.org/10.3389/fimmu.2018.01741

Smyth, D.J., V. Plagnol, N.M. Walker, J.D. Cooper, K. Downes, J.H. Yang, J.M. Howson, H. Stevens, R. McManus, C. Wijmenga, et al. 2008. Shared and distinct genetic variants in type 1 diabetes and celiac disease. *N. Engl. J. Med.* 359:2767–2777. https://doi.org/10.1056/NEJMoa0807917

Stark, R., T.H. Wesselink, F.M. Behr, N.A.M. Kragten, R. Arens, F. Koch-Nolte, K.P.J.M. van Gisbergen, and R.A.W. van Lier. 2018. T $_{RM}$ maintenance is regulated by tissue damage via P2RX7. *Sci. Immunol.* 3:eaau1022. https://doi.org/10.1126/sciimmunol.aau1022

Steinert, E.M., J.M. Schenkel, K.A. Fraser, L.K. Beura, L.S. Manlove, B.Z. Igyártó, P.J. Southern, and D. Masopust. 2015. Quantifying Memory CD8 T Cells Reveals Regionalization of Immunosurveillance. *Cell.* 161:737–749. https://doi.org/10.1016/j.cell.2015.03.031

Subramanian, A., P. Tamayo, V.K. Mootha, S. Mukherjee, B.L. Ebert, M.A. Gillette, A. Paulovich, S.L. Pomeroy, T.R. Golub, E.S. Lander, and J.P. Mesirov. 2005. Gene set enrichment analysis: a knowledge-based approach for interpreting genome-wide expression profiles. *Proc. Natl. Acad. Sci. USA.* 102:15545–15550. https://doi.org/10.1073/pnas.0506580102

ten Hoeve, J., M. de Jesus Ibarra-Sanchez, Y. Fu, W. Zhu, M. Tremblay, M. David, and K. Shuai. 2002. Identification of a nuclear Stat1 protein tyrosine phosphatase. *Mol. Cell. Biol.* 22:5662–5668. https://doi.org/10.1128/MCB.22.16.5662-5668.2002

Tessmer, M.S., C. Fugere, F. Stevenaert, O.V. Naidenko, H.J. Chong, G. Leclercq, and L. Brossay. 2007. KLRG1 binds cadherins and preferentially associates with SHIP-1. *Int. Immunol.* 19:391–400. https://doi.org/10.1093/intimm/dxm004

Todd, J.A., N.M. Walker, J.D. Cooper, D.J. Smyth, K. Downes, V. Plagnol, R. Bailey, S. Nejentsev, S.F. Field, F. Payne, et al.; Wellcome Trust Case Control Consortium. 2007. Robust associations of four new chromosome regions from genome-wide analyses of type 1 diabetes. *Nat. Genet.* 39:857–864. https://doi.org/10.1038/ng2068

Turner, D.L., C.L. Gordon, and D.L. Farber. 2014. Tissue-resident T cells, in situ immunity and transplantation. *Immunol. Rev.* 258:150–166. https://doi.org/10.1111/imr.12149

van Lint, A., M. Ayers, A.G. Brooks, R.M. Coles, W.R. Heath, and F.R. Carbone. 2004. Herpes simplex virus-specific CD8+ T cells can clear established lytic infections from skin and nerves and can partially limit the early spread of virus after cutaneous inoculation. *J. Immunol.* 172:392–397. https://doi.org/10.4049/jimmunol.172.1.392

Voehringer, D., C. Blaser, P. Brawand, D.H. Raulet, T. Hanke, and H. Pircher. 2001. Viral infections induce abundant numbers of senescent CD8 T cells. *J. Immunol.* 167:4838–4843. https://doi.org/10.4049/jimmunol.167.9.4838

Voehringer, D., M. Koschella, and H. Pircher. 2002. Lack of proliferative capacity of human effector and memory T cells expressing killer cell lectinlike receptor G1 (KLRG1). *Blood.* 100:3698–3702. https://doi.org/10.1182/blood-2002-02-0657

Wiede, F., B.J. Shields, S.H. Chew, K. Kyparissoudis, C. van Vliet, S. Galic, M.L. Tremblay, S.M. Russell, D.I. Godfrey, and T. Tiganis. 2011. T cell protein tyrosine phosphatase attenuates T cell signaling to maintain tolerance in mice. *J. Clin. Invest.* 121:4758–4774. https://doi.org/10.1172/JCI59492

Wiede, F., N.L. La Gruta, and T. Tiganis. 2014a. PTPN2 attenuates T-cell lymphopenia-induced proliferation. *Nat. Commun.* 5:3073. https://doi.org/10.1038/ncomms4073

Wiede, F., A. Ziegler, D. Zehn, and T. Tiganis. 2014b. PTPN2 restrains $CD8^+$ T cell responses after antigen cross-presentation for the maintenance of peripheral tolerance in mice. *J. Autoimmun.* 53:105–114. https://doi.org/10.1016/j.jaut.2014.05.008

Wiede, F., T.C. Brodnicki, P.K. Goh, Y.A. Leong, G.W. Jones, D. Yu, A.G. Baxter, S.A. Jones, T.W.H. Kay, and T. Tiganis. 2019. T-Cell-Specific PTPN2 Deficiency in NOD Mice Accelerates the Development of Type 1 Diabetes and Autoimmune Comorbidities. *Diabetes.* 68:1251–1266. https://doi.org/10.2337/db18-1362

Wiede, F., K.H. Lu, X. Du, S. Liang, K. Hochheiser, G.T. Dodd, P.K. Goh, C. Kearney, D. Meyran, P.A. Beavis, et al. 2020. PTPN2 phosphatase deletion in T cells promotes anti-tumour immunity and CAR T-cell efficacy in solid tumours. *EMBO J.* 39:e103637. https://doi.org/10.15252/embj.2019103637

Supplemental material

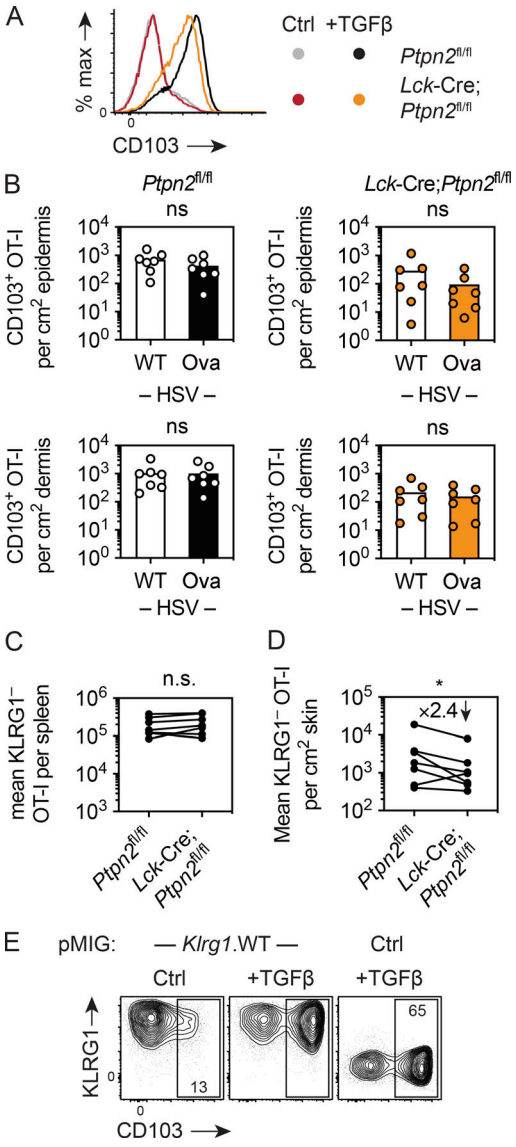

Figure S1. **Ptpn2 regulates early epidermal infiltration of OT-I cells independently of local antigen. (A)** In vitro activated *Ptpn2*$^{fl/fl}$ and *Lck-Cre;Ptpn2*$^{fl/fl}$ OT-I cells were cultured with IL-2 (25 U/ml) in the presence or absence (Ctrl) of TGFβ (10 ng/ml), as indicated. Analysis of CD103 expression 2 d after addition of TGFβ; data are representative of *n* = 2 experiments. **(B)** Enumeration of CD103$^+$ *Ptpn2*$^{fl/fl}$ (white) or *Lck*-Cre;*Ptpn2*$^{fl/fl}$ (orange) OT-I cells in epidermis and dermis in HSV-Ova (left flank)– and WT HSV (right flank)–infected skin 9 d after infection. Data were pooled from *n* = 2 experiments with *n* = 7 mice/group. **(C and D)** Means of KLRG1$^-$ OT-I cell numbers in spleen (C) and skin (D) from individual experiments 9 d after single or double HSV infection as in Fig. 1 H; data points from the same individual experiments (*n* = 7) connected by lines. Statistical significance (*, P < 0.05) determined by Wilcoxon test. **(E)** In vitro activated gBT-I cells transduced with pMIG.*Klrg1*.WT (left, middle) or pMIG.Ctrl (right) were cultured with IL-2 (25 U/ml) in the presence or absence (Ctrl) of TGFβ (10 ng/ml), as indicated. Analysis of KLRG1 and CD103 expression by GFP$^+$ gBT-I cells 3 d after addition of TGFβ; data are representative of *n* = 2 experiments.

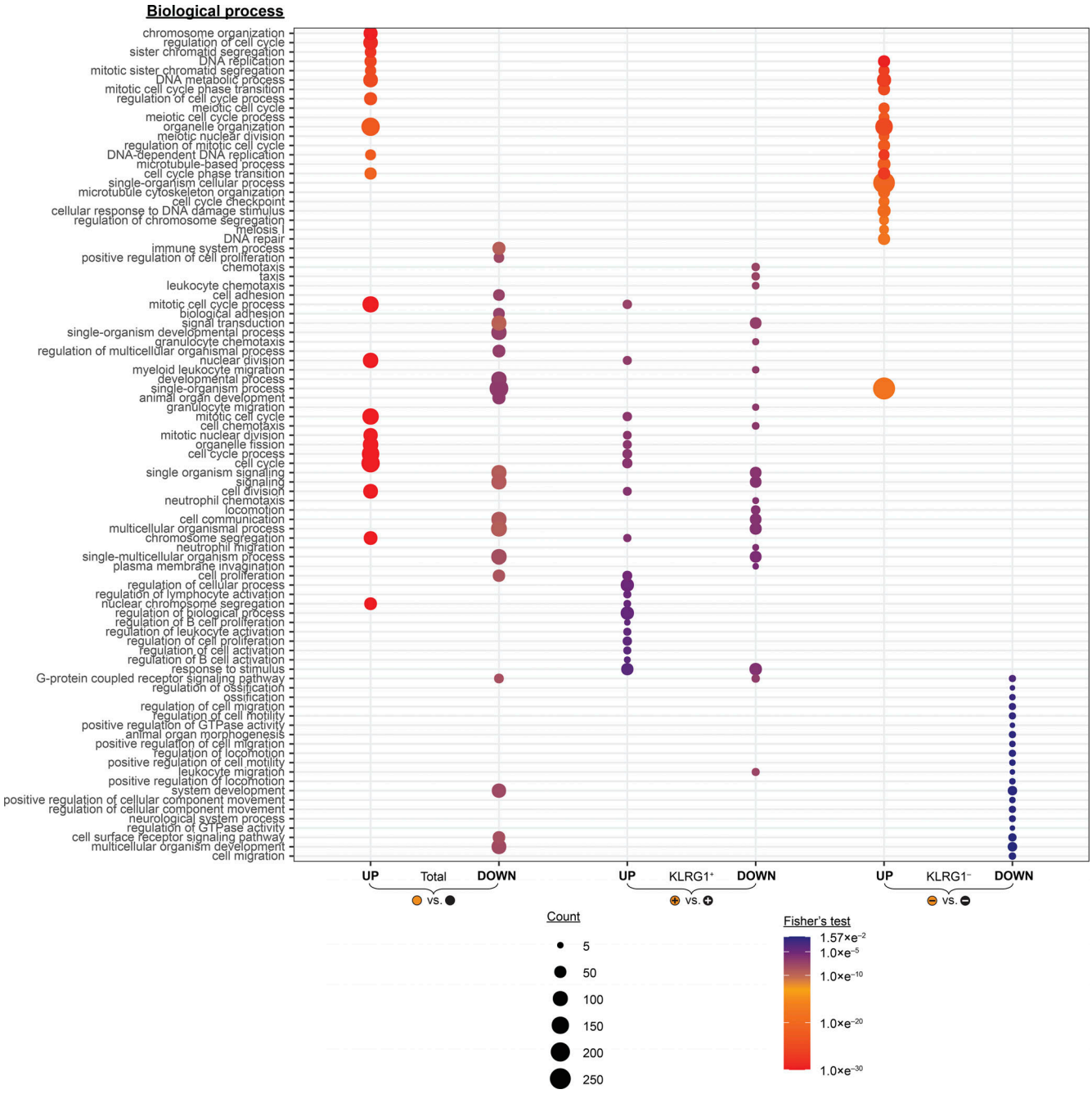

Figure S2. **List of significantly (P < 0.05) regulated biological processes (GO-term analysis) comparing transcriptional profiles of total (empty), KLRG1⁺ (+), and KLRG1⁻ (–) populations from *Ptpn2*$^{fl/fl}$ (black) and *Lck*-Cre;*Ptpn2*$^{fl/fl}$ (orange) OT-I cells.** Related to Fig. 3. Up to a maximum of 20 GO terms are shown per comparison. Dot size indicates number of genes in the respective cluster, with clusters of less than four DEGs removed from the analysis.

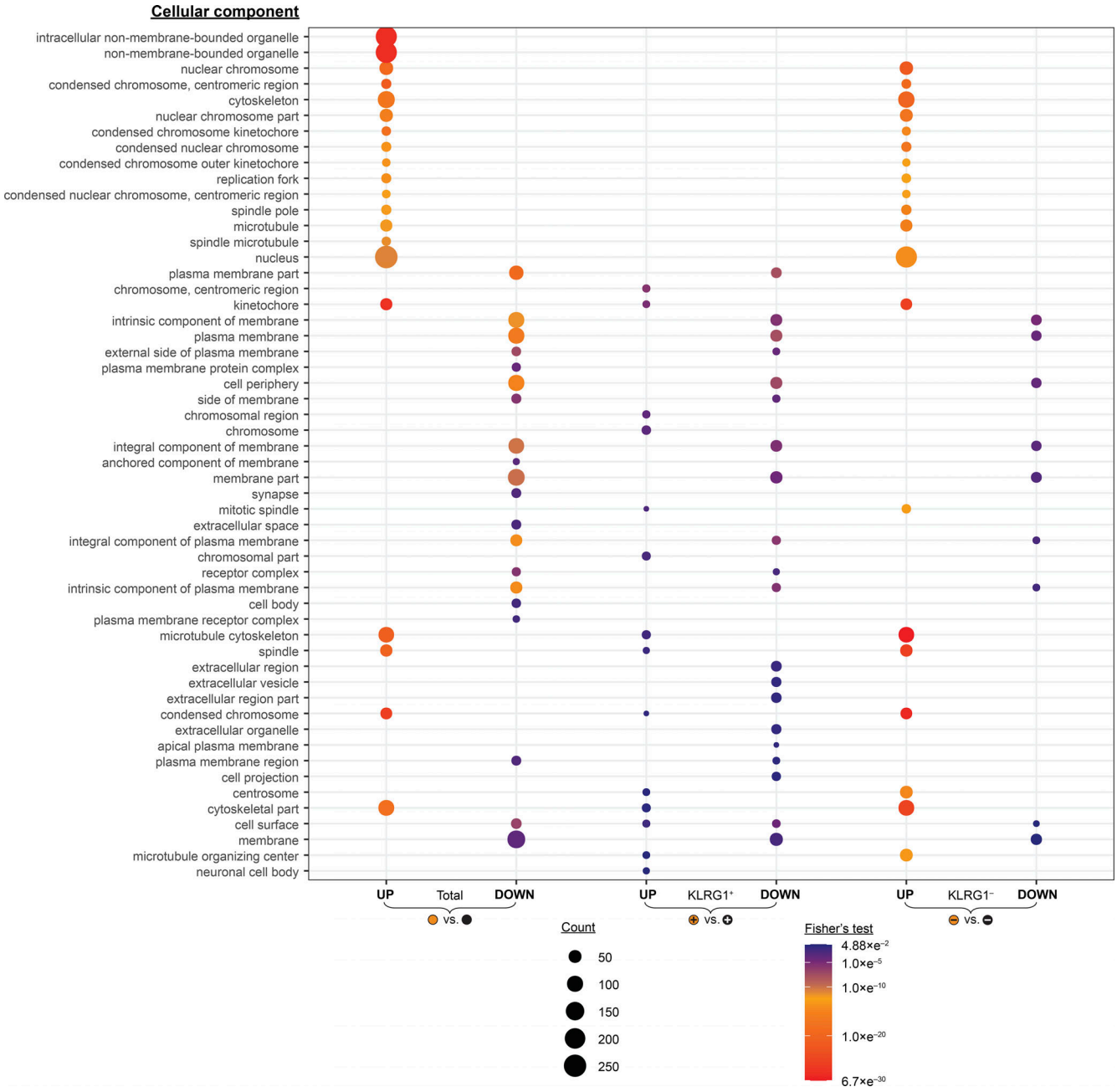

Figure S3. **List of significantly (P < 0.05) regulated cellular components (GO-term analysis) comparing transcriptional profiles of total (empty), KLRG1^{+} (+), and KLRG1^{-} (–) populations from *Ptpn2*$^{fl/fl}$ (black) and *Lck*-Cre;*Ptpn2*$^{fl/fl}$ (orange) OT-I cells.** Related to Fig. 3. Up to a maximum of 20 GO terms are shown per comparison. Dot size indicates number of genes in the respective cluster, with clusters of less than four DEGs removed from the analysis.

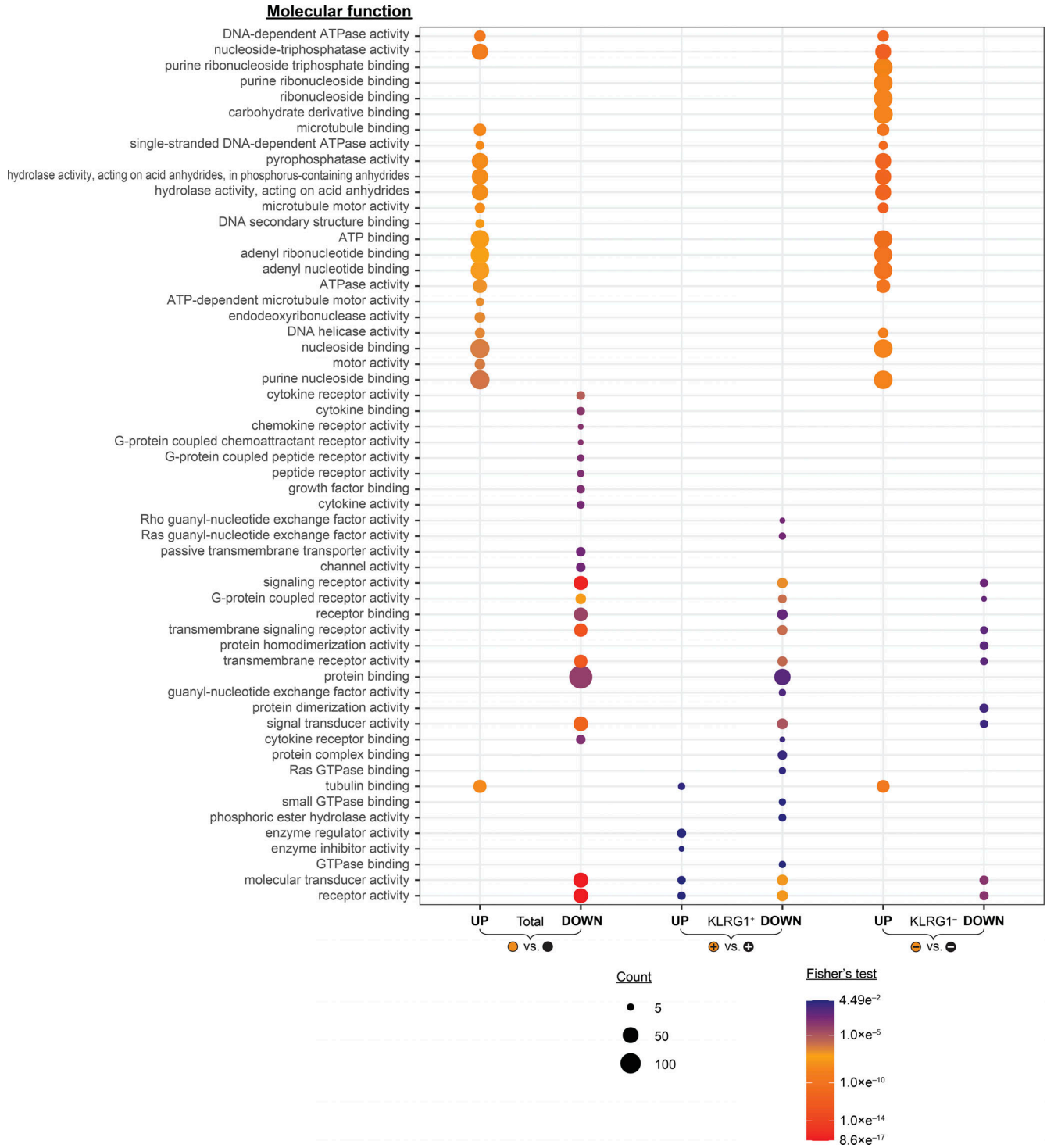

Figure S4. **List of significantly (P < 0.05) regulated molecular functions (GO-term analysis) comparing transcriptional profiles of total (empty), KLRG1^{+} (+), and KLRG1^{-} (–) populations from *Ptpn2*$^{fl/fl}$ (black) and *Lck*-Cre;*Ptpn2*$^{fl/fl}$ (orange) OT-I cells.** Related to Fig. 3. Up to a maximum of 20 GO terms are shown per comparison. Dot size indicates number of genes in the respective cluster, with clusters of less than four DEGs removed from the analysis.

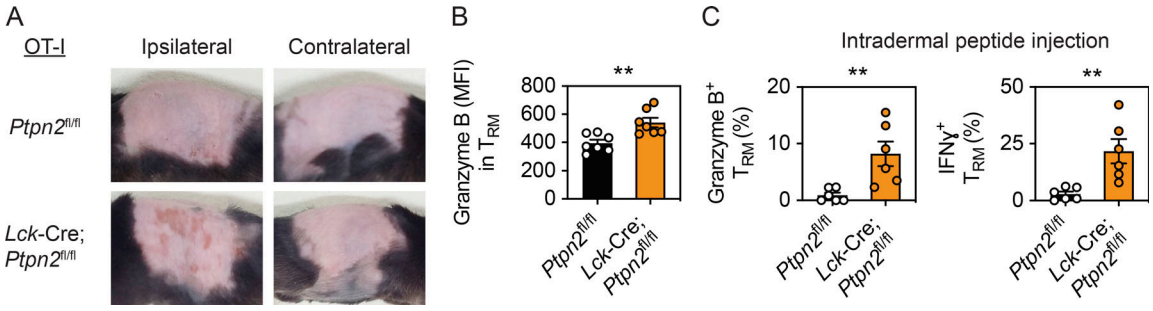

Figure S5. **Ptpn2 regulates T_{RM} effector functions. (A)** Representative photos of ipsilateral (left) and contralateral (right) flanks of *K5*-rTA;TetO.mOva mice 5 d after start of Dox treatment (1 mg/ml in drinking water). Mice received in vitro–activated *Ptpn2*$^{fl/fl}$ (top) and *Lck*-Cre;*Ptpn2*$^{fl/fl}$ (bottom) OT-I cells (5 × 10^6) by i.d. transfer >4 wk prior, as in Fig. 5 B. Photos depict whole flanks of mice. **(B)** Mean fluorescence intensity (MFI) for granzyme B–expressing *Ptpn2*$^{fl/fl}$ (black) and *Lck*-Cre;*Ptpn2*$^{fl/fl}$ (orange) T_{RM} cells in *K5*-rTA;TetO.mOva mice 5 d after start of Dox treatment (Fig. 5 D). Data pooled from *n* = 2 experiments with *n* = 7 mice per group. **(C)** Analysis of granzyme B and IFNγ expression by *Ptpn2*$^{fl/fl}$ (white) and *Lck*-Cre;*Ptpn2*$^{fl/fl}$ (orange) T_{RM} cells 6 h after i.d. injection of Ova peptide (SIINFEKL, 0.1 µg). Mice had received in vitro–activated OT-I cells (2 × 10^6) by i.d. transfer 4 wk prior, as in Fig. 4 C. *n* = 6 mice per group from one experiment. Statistical significance (**, P < 0.01) determined by Mann–Whitney test.

Three tables are provided online. Table S1 lists total *Lck*-Cre;*Ptpn2*$^{fl/fl}$ versus *Ptpn2*$^{fl/fl}$. Table S2 lists KLRG1$^+$ *Lck*-Cre;*Ptpn2*$^{fl/fl}$ versus *Ptpn2*$^{fl/fl}$. Table S3 lists KLRG1$^-$ *Lck*-Cre;*Ptpn2*$^{fl/fl}$ versus *Ptpn2*$^{fl/fl}$.